NAVAL POSTGRADUATE SCHOOL
Monterey, California

THESIS

RESPONSE OF AN ATMOSPHERIC PREDICTION MODEL TO TIME-DEPENDENT SEA-SURFACE TEMPERATURES

by

Peter Henry Ranelli

March 1984

Thesis Advisor: R. L. Elsberry

Approved for public release; distribution unlimited.

REPORT DOCUMENTATION PAGE

READ INSTRUCTIONS BEFORE COMPLETING FORM

1. REPORT NUMBER

2. GOVT ACCESSION NO.

3. RECIPIENT'S CATALOG NUMBER

4. TITLE (and Subtitle)

Response of an Atmospheric Prediction Model to Time-Dependent Sea-Surface Temperatures

5. TYPE OF REPORT & PERIOD COVERED
Master's Thesis; March, 1984

6. PERFORMING ORG. REPORT NUMBER

7. AUTHOR(s)

Peter Henry Ranelli

8. CONTRACT OR GRANT NUMBER(s)

9. PERFORMING ORGANIZATION NAME AND ADDRESS

Naval Postgraduate School
Monterey, California 93943

10. PROGRAM ELEMENT, PROJECT, TASK AREA & WORK UNIT NUMBERS

11. CONTROLLING OFFICE NAME AND ADDRESS

Naval Postgraduate School
Monterey, California 93943

12. REPORT DATE
March 1984

13. NUMBER OF PAGES
112

14. MONITORING AGENCY NAME & ADDRESS(if different from Controlling Office)

15. SECURITY CLASS. (of this report)
Unclassified

15a. DECLASSIFICATION/DOWNGRADING SCHEDULE

16. DISTRIBUTION STATEMENT (of this Report)

Approved for public release; distribution unlimited.

17. DISTRIBUTION STATEMENT (of the abstract entered in Block 20, if different from Report)

18. SUPPLEMENTARY NOTES

19. KEY WORDS (Continue on reverse side if necessary and identify by block number)

Atmosphere-Ocean Coupled Models
T-EOTS
Sea Surface Temperature
NOGAPS

20. ABSTRACT (Continue on reverse side if necessary and identify by block number)

The purpose of this research is to explore the need for time-dependent sea-surface temperatures in atmospheric model predictions up to 10 days. The Navy Operational Global Atmospheric Prediction System is used in this study. First, a control run is made in which the sea-surface temperature (SST) is fixed in time. In the test case, the observed SST analyzed each 12 hours by the Fleet Numerical Oceanography Center are used to

#20 - ABSTRACT - (CONTINUED)

force the system. The 10-day predictions are compared to determine if a coupled atmosphere-ocean model would improve or deteriorate the atmospheric predictions. The case analyzed occurred after the oceanic spring transition so that only small increases in SST occurred. Use of time-dependent SST resulted in only small changes in latent, sensible and total heat fluxes, and in storm tracks and intensities. Thus, further case studies of the atmospheric response are necessary to indicate whether coupled atmosphere-ocean models are required on 10-day time scales.

Approved for public release; distribution unlimited.

Response of an Atmospheric Prediction Model to Time-Dependent Sea-Surface Temperatures

by

Peter Henry Ranelli
Lieutenant Commander, United States Navy
B.S., Rensselaer Polytechnic Institute, 1975

Submitted in partial fulfillment of the
requirements for the degree of

MASTER OF SCIENCE IN METEOROLOGY AND OCEANOGRAPHY

from the

NAVAL POSTGRADUATE SCHOOL

March 1984

ABSTRACT

The purpose of this research is to explore the need for time-dependent sea-surface temperatures in atmospheric model predictions up to 10 days. The Navy Operational Global Atmospheric Prediction System is used in this study. First, a control run is made in which the sea-surface temperature (SST) is fixed in time. In the test case, the observed SST analyzed each 12 hours by the Fleet Numerical Oceanography Center are used to force the system. The 10-day predictions are compared to determine if a coupled atmosphere-ocean model would improve or deteriorate the atmospheric predictions. The case analyzed occurred after the oceanic spring transition so that only small increases in SST occurred. Use of time-dependent SST resulted in only small changes in latent, sensible and total heat fluxes, and in storm tracks and intensities. Thus, further case studies of the atmospheric response are necessary to indicate whether coupled atmosphere-ocean models are required on 10-day time scales.

TABLE OF CONTENTS

LIST OF FIGURES

ACKNOWLEDGEMENTS

I would like to express my sincere gratitude to Professor R. L. Elsberry for assistance and guidance during this research. The time and effort that Dr. T. E. Rosmond always had available to assist me with running NOGAPS has been greatly appreciated. Dr. T. Tsui and Mr. P. Harr provided considerable aid, expertise and support which made my work more pleasurable. Finally, I would like to thank LCDR S. A. Sandgathe, who provided the initial inspiration and continuing motivation during this project.

I. INTRODUCTION

It is well known that important interactions between the atmosphere and the ocean exist on time scales of a month or longer. The interaction between the atmosphere and the ocean on shorter time scales is less well understood. However, heat fluxes from the ocean into the atmosphere are believed to play an important role in many atmospheric circulations.

Rapid advancements in the last three decades have greatly improved both the quality and the speed of numerical weather prediction models. Presently, the accuracy of the model forecast decays as the forecast time increases and the forecasts are, in general, no better than climatology after five or six days. To improve model forecasts beyond this present limitation, some type of feedback between the atmosphere and the ocean most likely will be required.

This thesis is the first in a series of case studies designed to study the necessity and feasibility of coupling an atmospheric model and an oceanic model. The techniques for running an atmospheric model with a time-dependent sea-surface temperature (SST) were developed and then used to make two atmospheric model prediction runs. One was a control run in which the SST was held constat, as is presently done in operational models. In the second model run, a

time-dependent SST was used to simulate a coupled air-ocean model. Actual SST analyses were used in this "perfect-prog" approach. The changes in surface heat fluxes were then analyzed.

The following chapters describe the experiment and the changes in the model response between the two model runs. Chapter II is background on the scientific considerations for this experiment. Chapter III is an explanation of the experiment design including a brief description of the atmospheric model used. Chapter IV is the analysis of the changes in the heat flux. Chapter V analyzes the changes in this cyclogenesis as forecast by the two model runs and compared to the actual storm development. Chapter VI contains the conclusions reached in this study and recommendations for further study.

II. BACKGROUND

The theoretical limit of predictability of numerical weather prediction is on the order of 15 days [Rosmond et al., 1983]. To improve from present forecast capability of perhaps three to five days to the theoretical limit will require a large amount of effort and research. Many problems stand in the way of the researcher attempting to reach this goal. A nearly perfect numerical model will be required before a 15-day forecast can be attained. More complete understanding of many atmospheric processes and many improvements to available models will be required.

During the short time scales, atmospheric changes on a synoptic scale are mainly a result of dynamical forcing. The barotropic and baroclinic processes of the atmosphere which are the main contributors to the dynamical forcing are well represented in numerical models. The forecast problem on the short time scale is then one of correctly initializing the numerical model and then integrating the initial conditions forward in time. For the medium range (5-15 day) time scales, external forcing of the atmosphere, such as diabatic processes become increasingly important in determining the atmospheric response. In the 15-30 day range, the forecast problem becomes less of an initial value problem and more a problem in which the external forcing and/or the

diabatic processes begin to dominate the predicted circulations. Diabatic processes are in turn forced by external factors such as the oceanic heat source.

A. THE AIR-SEA INTERACTION PROBLEM

There are many sources and sinks of heat in the atmosphere, including latent heat release, solar radiation, longwave radiation and the heat fluxes across the air-sea interface. Air-sea interaction becomes an important physical process that has to be modelled on 15-day time scales. Sandgathe (1981) has concluded that numerical model forecasts of maritime cyclogenesis require an accurate specification of the air-sea fluxes. All fluxes across the air-sea interface can be modelled as a function of the sea-surface temperature (SST). It is the hypothesis of this study that a sophisticated model capable of forecasting on a 5-15 day time scale will require a time-dependent SST. Without this time-dependent SST, representation of the interface fluxes may be inaccurate and this will deteriorate the forecast.

There are many oceanic processes that can cause significant changes in the SST on 10-day time scales and result in a response in the atmospheric model. Large changes in SST can occur during the spring and autumn transition periods in the ocean. During this period, there are warm and shallow ocean mixed layers that may deepen and cool rapidly in response to atmospheric forcing [Camp and Elsberry, 1978; Elsberry and Camp, 1978; Elsberry and Raney, 1978]. During

winter, the ocean mixed layer is deeper and the changes in SST due to winter storms are smaller. Summer storms are less intense than winter storms and do not force a large change in the SST.

Western ocean boundary current regions, such as the Kuroshio and the Gulf Stream, are prime areas of cyclogenesis [Sanders and Gyakum, 1980]. These ocean current features meander eastward after departing from the east coast of continents. Locations of the associated SST gradients will be important in determining the atmospheric response to these features.

Equatorial regions may also experience significant changes in SST, which alter the surface heat flux and the amount of deep convection in this region. This response is felt in less than one day in the lower troposphere and, in special circumstances, can affect the long waves of the mid-latitudes within seven days.

An oceanic forecast model would be required to provide the time-dependent SST to force an operational atmospheric model. While the oceanic model might be run independently to generate the SST, it is assumed that the atmospheric model might provide important feedback to the oceanic model. Therefore, a coupling of the two models might be required to provide the best forecasts both in the atmosphere and the ocean.

B. U.S. NAVY ROLE/REQUIREMENTS

Environmental factors both in the air and the ocean will be an important consideration in many decisions made by operational commanders. On a short time scale, immediate operations such as flight operations from an aircraft carrier or an underway replenishment may be affected. The ability of anti-submarine warfare operators to find a submarine or the submarine's ability to avoid detection is always very dependent on knowledge of the thermal structure of the ocean and the resulting acoustical propagation paths. Long range plans, such as an ocean crossing, planning for an amphibious landing, or a major fleet exercise could be closely linked to environmental considerations.

Modern weapon systems are becoming more sophisticated and complex. Environmental conditions are an important factor in the development and operational application of these systems. During the weapon development, climatological variations are often used for design purposes. When these weapon systems are deployed, their effective utilization requires an accurate and complete forecast of the actual atmospheric variations to be encountered.

The Fleet Numerical Oceanography Center (FNOC) and the Naval Environmental Prediction Research Facility (NEPRF) recognized the need to improve medium-range forecasts and began a study of the feasibility of developing a coupled atmospheric-oceanic model in early 1982. The goal was to

eventually provide an accurate forecast of both the ocean and the atmosphere for a 15-day period. The studies by Elsberry et al., (1982) and Rosmond et al., (1983) concluded that additional research is required before the FNOC atmospheric forecast is extended beyond five days, or before an atmospheric model and an oceanic model are coupled. The question explored here is whether a viable forecast beyond five days requires a time-dependent SST, which might be provided by a coupled air-ocean model. Before a coupled model becomes operationally useful, the sensitivity of the atmospheric model to the air-sea interaction must be understood.

C. COUPLED ATMOSPHERE-OCEAN MODELS

Previous studies regarding coupled models have mainly focused on the climatological effects of a changing SST on the atmosphere. These studies are mainly concerned with the atmospheric response over months or years. A comprehensive review of these studies was done by Elsberry et al., (1982).

Arpe (1981) has examined the sensitivity of an atmospheric model to a different SST field on short to medium range time scales. Arpe worked with the ECMWF model, which presently uses the climatological SST to calculate surface fluxes. Arpe substituted large scale temperature anomalies, some with values as high as 3°C, into the model. The sea-surface temperature anomalies were fixed in time. He showed that forecasts beyond six days were sensitive to large scale SST

anomalies. He also showed higher SST values in a region resulted in a more rapid and intense development of cyclones.

This study is the first in a series of case studies designed to evaluate what effects a coupled atmosphere-ocean model may have on an atmospheric prediction in the medium-range forecast periods. Rather than using an oceanic model to provide the time-dependent SST, the actually observed SST evolution will be specified. This "perfect prognosis" of specifying the SST avoids any errors which might be introduced by an ocean model. Studies of the atmospheric response and feedback processes using "perfect-prog" SST forcing is essential to identify potential atmospheric model-dependent problems before full interaction of the two models is attempted. By avoiding errors that might result from biases in the oceanic model, the analysis of the atmospheric model response is made simpler.

D. COUPLING SCHEMES

Three methods have been described by Elsberry et al., (1982) for coupling an atmospheric model to an oceanic model. The methods are, in increasing sophistication, minimal feedback or weak coupling, non-synchronous coupling and synchronous coupling (Fig. 1). The coupling strategies must take into account the inherent differences in the time steps of an atmospheric model and an oceanic model. Atmospheric models normally have an advective time step on the order of five minutes, with the calculation of diabatic effects every 30

to 40 minutes. Oceanic models have a time step on the order of one hour.

The simplest coupling scheme is the minimal feedback type of coupling (Fig. 1a). For this type of coupling, the analyzed SST field at the initialization time of the atmospheric model is used as input for the model initial conditions. The SST then remains constant for the entire model run. This type of coupling is used in present operational models. Beyond five-day forecast periods, air-sea interaction plays an increasing role in the atmospheric response and this type of coupling may not prove accurate for medium range forecasts.

The second method is non-synchronous coupling (Fig. 1b). In this case, a SST prediction for the entire forecast period is assumed to be available and is used as input during the appropriate times in the atmospheric model runs. The time-dependent SST can be provided from either an ocean model forecast that has been run independently of the atmospheric model or from analyzed SST fields in a "perfect prog" hindcast. This method provides a more realistic representation during periods of changing physical conditions than does the weakly coupled method. The non-synchronous method may be impractical for operational use if an independently-run ocean prediction develops biases which would overwhelm a forecast by the atmospheric model during a 10-15 day forecast. However, this type of coupling is an excellent research tool when using the "perfect-prog" SST fields.

The final and most sophisticated scheme is the fully synchronous coupling (Fig. 1c). The two models are run concurrently and provide feedback to each other at the appropriate point in the model integration. In this way, the SST used in the atmospheric model and the atmospheric forcing (surface wind, surface heat fluxes, precipitation) for the oceanic model are being continually updated. While this is obviously the most complicated of the three schemes, it should also provide the best forecast. Only a fully synchronous coupled atmospheric-oceanic model should provide a 15-day forecast capability [Rosmond et al., 1983].

In summary, the goal of this research is to determine the atmospheric forecast model response to a time-dependent SST. The study was conducted using a non-synchronous coupling with "perfect-prog" SST to isolate the atmospheric response. By studying the response in this type of model, understanding of the role of air-sea interaction can be improved. This better understanding of the model air-sea interface processes should then ultimately lead to a fully synchronous coupled model.

III. PROCEDURE

An experiment was designed to examine the sensitivity of an atmospheric prediction model to time-dependnet sea-surface temperatures (SST). The model chosen for this experiment was the Navy Operational Global Atmospheric Prediction System (NOGAPS). Time-dependent sea-surface temperatures were obtained from the Fleet Numerical Oceanography Center (FNOC) twice-daily analyses.

The experiment was straightforward in design. Two model runs to ten days forecast time were made with NOGAPS. In the first run, designated the control run, the SST was held constant as captured in the initial conditions. In the second run, designated the SST run, the SST were updated every twelve hours. The model atmospheric response in each of the two runs was then analyzed for changes. Specifically, the changes in the intensity of cyclogenesis and storm tracks were examined.

A. NAVY OPERATIONAL GLOBAL ATMOSPHERIC PREDICTION SYSTEM (NOGAPS)

NOGAPS is the Navy's state-of-the-art atmospheric prediction model. The model was made available by Dr. T. Rosmond of NEPRF. The version of NOGAPS used in this experiment contains all modifications made to the system through July 1983.

The NOGAPS forecast model is a six-layer, sigma coordinate, primitive equation model. It is based upon the UCLA

general circulation model (GCM), described by Arakawa and Lamb (1977). The diabatics of the model are of full GCM sophistication. NOGAPS includes the parameterization of the planetary boundary layer (PBL) after Randall (1976) and Deardorff (1972); cumulus convection using the Arakawa-Schubert (1974) scheme; and radiation as described by Katayama (1972) and Schlesinger (1976). It should be noted that NOGAPS differs from the UCLA GCM in that the PBL is not allowed to exceed the first sigma level. This effectively limits the PBL to the bottom 200 mb of the atmosphere. A more complete description of NOGAPS is contained in Appendix A.

The extremely complete package of diabatic processes used in the model was felt to be an important consideration in the selection of NOGAPS for this experiment. The full parameterization of both the PBL and the cumulus convection was necessary for the effects of the changing SST to be felt in the rest of the model. Without full diabatics, the response to the SST would have been diminished. Before a fully synchronous coupled air-ocean model becomes operational, the boundary layer physics in both the atmosphere and the ocean, as well as the interaction between the two, will have to be more fully understood. This experiment is just one step toward that goal.

B. SEA-SURFACE TEMPERATURES

The time-dependent SST used in this experiment were obtained from FNOC. FNOC performs SST analyses twice daily

at 0000 GMT and 1200 GMT. The analysis is an integral part of the Thermal Ocean Prediction System-Expanded Ocean Thermal Structure (TOPS-EOTS). TOPS is a synoptic, mixed layer forecast model. EOTS is an ocean thermal analysis procedure which uses information blending techniques to blend XBT and surface ship reports to a three dimensional grid. Satellite-derived SST reports are not presently used in the analysis. The combined TOPS-EOTS had only been in an operational status a few months when the NOGAPS initial conditions and SST were captured. However, in a four-month study the TOPS-EOTS combination had less noise in the daily analysis than the conventional EOTS [Clancy and Pollack, 1983]. A more complete description of the TOPS-EOTS system can be found in Appendix B.

Observed sea-surface temperatures were used in the experiment to substitute a "perfect-prog" of an ocean model. A case study with non-synchronous coupling of the models, using a "perfect-prog" forecast of the SST, is a test to isolate atmospheric model dependent errors [Rosmond, et al., 1983]. The effect of variations in model-predicted SST would be enough to cause changes in the atmospheric response. By using the observed SST in a "perfect-prog," these oceanic model errors could be removed and attention focused in the atmospheric model response to changing SST. It is felt that if an atmospheric model does not respond to the SST changes in a "perfect" ocean model, then it is unlikely that coupled

atmospheric-ocean models would be required on 7-10 day time scale.

C. INITIAL CONDITIONS

The initial conditions used to make the model runs for this experiment were captured at the time of the FNOC operational forecasts. Four different sets of initial conditions were captured in late April and May of 1983. Initial conditions had to be captured in real time at multiple time periods for several reasons. First, to simulate an actual operational forecast it was necessary to obtain the initial conditions used by FNOC at the time of the actual forecast. A delay in obtaining the initial conditions would have the advantage of increasing the number of observations used to determine the initial conditions. This would have improved the initial conditions for the model and resulted in a better forecast. However, it would have partially destroyed the objectives of this experiment which were to determine the sensitivity of an operational forecast model to time-dependent SST. Second, the NOGAPS analysis, data assimilation and prediction model require a several day period to stabilize after the model is restarted. This "spin-up" period allows internal gravity waves and other imbalances to filter out of the initial fields used. After this "spin-up" period the model forecast fields are much smoother.

The time period was chosen to coincide with the occurrence of the spring transition period in the ocean. During

the transition, large changes in the SST are possible due to the rapid shallowing of the mixed layer. However, it was desirable to select a period before the seasonal thermocline had become very strong. The atmospheric analyses were monitored for occurrences of cyclogenesis and a storm track across a large portion of the Pacific Ocean. If this occurred, the increased mixing due to the increased surface wind stress could act to mix through the incipient seasonal thermocline and rapidly deepen the mixed layer. The increased mixing would reduce the SST due to the entrainment of cold water into the mixed layer. In the atmospheric model runs with the time-dependent SST, the reduced SST should act to impede the cyclogenesis compared to the control run.

Given these constraints, the most favorable conditions for a model run appeared in the Pacific Ocean in late May. The initial conditions captured were for 1800 GMT 26 May 1983. This was a NOGAPS 6-hour update and not an actual forecast. Since this was a full initialization for a NOGAPS forecast, this should not have caused a problem in the experimental forecasts.

In capturing the SST fields for this ten-day period, the TOPS-EOTS analysis was not available from the 0000 GMT 3 June analysis to the end of the 10-day forecast at 1800 GMT 5 June 1983. The lack of a changing SST for the last three days of the forecast period may cause some differences in the overall final forecast. However, three days is too

short a period for a significant effect on the model. Thus, the major goal of being able to compare the effect of time dependent SST on two model runs could still be obtained.

D. EXPERIMENTAL PROCEDURES

In the control run from 1800 GMT 26 May 1983, the SST were held fixed at the initial values, as is presently done in the operational forecasts. The model was integrated to ten days (rather than five days as is the case of the operational forecasts) with no changes in any of the input initial fields (Fig. 2a). A complete history tape was written every six hours during the model run for future analysis. These fields include the winds, heights, humidities and temperatures for several levels. Various PBL parameters were output as well, including the total heat flux, moisture (latent heat) flux, sensible heat flux and long and short wave radiative heat fluxes. Precipitation fields associated with cumulus convection and large scale lifting were also output.

The second model run, designated the SST run, was made using the "perfect-prog" time-dependent SST. The new SST were input every 12 h at 0000 and 1200 GMT during the forecast (Fig. 2b). No time interpolation of the SST fields to smooth the effect of the change was performed. The last of the changing SST was input at 162 h and held constant for the remainder of the integration. A similar history tape was generated from the SST run as for the control run.

IV. HEAT FLUX ANALYSIS

The surface fluxes of sensible and latent heat in NOGAPS are parameterized according to Deardorff (1972) based on the sea-surface temperature and the values of T and q from the dynamic portion of the model. The surface heat fluxes are then used to force the remainder of the diabatic processes in the model. The first changes in the model response to the time-dependent SST will be seen in the surface heat fluxes. This chapter analyzes the SST changes during the SST run and the resulting changes in the surface heat fluxes. The next chapter considers the effects of these changes on the overall synoptic pressure patterns, specifically the changes in cyclogenesis and storm tracks.

A. SEA-SURFACE TEMPERATURE CHANGES

The initial SST fields (Fig. 3) are from the TOPS-EOTS analysis at 1200 GMT 26 May 1983. This field has a predominant north-south gradient with very little structure, except along the coastal regions. The warmest areas of 26°C are found in the southwestern corner of the ocean basins while the coldest regions of -1°C are found in the northwestern corner of the basins.

The Pacific Ocean SST field shows the Kuroshio current as a strong gradient along the east coast of Japan. Along the west coast of North America, a plume of warm water extends

northward into the Gulf of Alaska. South of this feature, the southward flowing eastern boundary current has resulted in lower SST along the coast. The gradient is not as strong as along the western boundary.

In the Atlantic Ocean, the predominant gradient is oriented NW-SE over most of the ocean north of 40°N due to the strong influence of the Gulf Stream. The Gulf Stream is evident as a strong gradient extending from the east coast of the U.S. to the northeast above Great Britain. The structure of the Gulf Stream in this analysis begins at 35°N and not in the Florida straits as expected.

The differences between the SST fields used as input to the SST run and the initial SST were computed to determine the horizontal variations of the changes in the SST field. These differences were analyzed at 24-h intervals to remove any diurnal effects. The 0000 GMT analyses for each day were used to observe the first change in SST. However, this selection did introduce a diurnal effect between the time-dependent SST fields and the initial SST at 1800 GMT 26 May 1983. It is most evident along the edges of continents, since the diurnal surface temperature change is much greater over continents than over the ocean surface. The changes over the land have been shaded out in the following figures, but the land effect can be seen as a strong gradient near the coastal boundaries.

The first change in the SST field was inserted at six hours of the model run. Changes in SST (Fig. 4) are generally

less than 0.5°C. In the Pacific Ocean, the changes are in north-south bands of alternating cooling and warming regions. The largest temperature change of 2°C is found in the region of the Kuroshio. In the Atlantic, there is a cooling along the east coast of North America, with changes as large as 2°C. The area of cooling extends eastward into the middle of the basin. Large areas of lower SST are also found in the southern part of the basin and over most of the northern area. Changes in these two areas are generally less than 0.5°C. Warming occurs over most of the eastern Atlantic with small regions extending to the area north of Cuba.

The SST input at 30 h had larger departures from the initial field (Fig. 5). Large areas of 0.5°C temperature change can be seen as well as some areas of 1.0°C change in the middle of the basin. A warming trend, especially in the Atlantic Ocean, is evident as the area of positive temperature changes increases.

The 54-h SST change (Fig. 6) continues the trend to higher temperatures. The area of lower temperatures in the region of the Kuroshio and the Gulf Stream has begun to shrink. Most of the Pacific basin has temperature differences of less than 0.5°C. The only exception is a large area of temperature decreases exceeding -1.0°C in the southeastern part of the basin. The Atlantic is also warmer. The only region of lower temperatures is in the center of this basin.

The SST changes for 78 h (Fig. 7), 102 h (Fig. 8), and 126 h (Fig. 9) continue the warming trend that has been

occurring over most of both ocean basins. The Kuroshio area temperatures increase rapidly during this period and has differences as large as +2.0°C. There is a second area of maximum temperature increases in the middle of the Pacific basin. The area of temperature decrease in the eastern Pacific is still present with almost the same areal coverage of previous times. However, the magnitude of the changes is decreasing. In the Atlantic near the Gulf Stream, a center of temperature increase replaces most of the previous area of temperature decrease. Maximum increases of 2.0°C are found in this area of the Gulf Stream and in the area to the northeast of Cuba. The largest change is at 102 hours, when a 2.5°C change is analyzed in the region to the north of Cuba. The area of small temperature decreases in the central Atlantic Ocean remains approximately constant. At 126 h, this area begins to shrink but the central value is larger in magnitude.

The final SST field analyzed was input to the model at 150 h. At this time, changes in the SST field (Fig. 10) had resulted in a much warmer ocean surface than the initial SST field. Most of the western Pacific Ocean has a temperature increase of at least 0.5°C with large areas over 1.5°C. The area of temperature decrease has become smaller than 24 h previously and is now mainly located in the southeastern part of the basin. A separate area of small temperature decreases is also present south of the Aleutian Islands. The Gulf Stream area has warmed significantly. Most of the area

of temperature decrease along the east coast of the U.S. has disappeared. The largest temperature increases of 2.0°C are found in the northern region of the Atlantic basin. Most of the Atlantic has warmed a minimum of 0.5°C with large areas over 1.0°C. The area of temperature decreases in the center of the Atlantic has remained throughout this period.

The final SST field was input at 162 h of the model run. Thus, the changes for 150 h are representative of the changes for the rest of the model run.

Since an area may have both positive and negative departures relative to the initial SST during the integration, it is difficult to summarize the SST changes. One method of establishing a trend would be to take the 150 h SST departures and divide by 7.25 days. The method used in this study was to take the simple sum of the seven daily SST departures from the initial value. The sum of the 24-hour SST changes (Fig. 11) shows the areas of total SST increases and decreases to the model. In general, the cumulative temperature departures over the Pacific Ocean have positive values of 2.5°C over much of the basin. Lower temperatures are seen along the coasts of both continents and in a large region of the eastern Pacific. The Atlantic Ocean has a similar change. A large area of temperature decrease is in the center part of the Atlantic Ocean, but the magnitude of the total change is less than 2.5°C. Along the east coast of the U.S. is a second area of large temperature decrease. The rest of the

basin has a temperature increase with the largest magnitudes in the southwestern corner and in the north of the basin.

In summary, the SST departures showed a general warming trend over much of the two ocean basins. There were also areas of lower SST's in both oceans. The magnitude of the positive SST changes was almost double that of the negative temperature departures. Lower SST values occurred during the first four days along western boundaries of both oceans. However, temperature increases occurred in this area in the last SST input, which was maintained for the last 78 h of the integration.

B. SURFACE HEAT FLUX CHANGES

The surface heat fluxes (sensible, latent and total) are responsive to changes in the SST. The surface fluxes are analyzed here to determine the direct effect that a time-dependent SST had on the model. Subsequent changes in the atmospheric model will depend on how efficiently these fluxes are transported from the surface via the PBL to the free atmosphere. In this regard, a model with higher vertical resolution than the six-layer version of NOGAPS used in this study will probably improve the model response to a time-dependent SST.

The analysis consisted of determining the mean and standard deviation for each run for the sensible, latent and total heat fluxes. The mean and standard deviation were computed over the 40 six-hourly calculations. The difference

of the two model runs was then determined to illustrate the change in model response. In the following figures upward heat flux (from the ocean to the atmosphere) is positive. A positive number in the difference fields indicates less heat flux was available to the atmosphere in the SST run.

1. Sensible Heat Flux

The sensible heat flux is dependent on the air-sea temperature difference rather than just the SST. A higher SST may not result in an increased sensible heat flux if the air temperature also increases and results in a smaller air-sea temperature difference. Sensible heat flux is the smallest of the three heat fluxes analyzed here.

The sensible heat fluxes for the Pacific Ocean (Fig. 12) and the Atlantic Ocean (Fig. 13) show upward sensible heat flux over most of the ocean basins for both model runs. Areas of downward heat flux (indicating the air is warmer than the ocean surface) are found along the western edge of the Pacific Ocean extending southeastward from Kamchatka as far as 30°N. This southeastward extension is slightly less in the SST run. An area of negative fluxes is also found in the northeastern Pacific Ocean. The magnitude of the flux is much smaller in the SST run. The only area of net downward heat flux in the Atlantic Ocean is in the northwestern portion of the basin which is also the area of lowest SST. The effect of the Gulf Stream is very evident as the maximum upward flux extends from the east coast of the U.S. to the northeast

and into the center part of the Atlantic. Fluxes in the Atlantic are larger than 6 gm-cal/cm^2-hr as opposed to the largest flux of 3 gm-cal/cm^2-hr in the Pacific.

In the Pacific Ocean, the change in the flux very clearly follows the change in SST (Fig. 11). Areas of higher SST have resulted in a positive change in the flux and large changes in the SST correlate with large changes in flux. An exception is the area of the Pacific centered at 30°N, 180°. This is the area of highest SST change but the corresponding heat flux change is not large. This suggests the air temperature had also increased and resulted in a lower air-sea temperature difference than expected. The Atlantic Ocean sensible heat flux difference also closely follows the changes in SST.

For both basins, the change in sensible heat flux was small compared to the mean values for the forecast period. Largest changes of 1.5 gm-cal/cm^2-h in the Pacific Ocean and 0.5 gm-cal/cm^2-h in the Atlantic Ocean occurred along the east coast of continents. This is most likely due to the higher temperatures associated with western boundary currents than with the rest of the ocean.

The standard deviation of the sensible heat flux for the Pacific Ocean (Fig. 14) and the Atlantic Ocean (Fig. 15) are of the same magnitude as the mean values. The contours generally follow the pattern of the mean field. Largest variations are associated with the western boundary currents.

The large variation in flux is most likely due to the passage of cyclones along the area of largest SST gradient. In advance of a cyclone there is zero or downward heat flux while there are large upward fluxes behind the cold front. The fluctuations in heat flux can be associated with the pattern of warm advection in advance and cold advection behind the cold front.

The difference of the standard deviations for the two model runs shows very little change for the central and eastern part of the oceans. A large increase in the amount of variation in the SST run near the western boundary currents can be seen. The changes in SST are consistent with a higher standard deviation in the SST run.

2. Latent Heat Flux

The transfer of water vapor across the air-sea interface results in a transfer of energy due to the latent heat of evaporation required to evaporate the water. The latent heat flux is proportional to the difference between the saturation vapor pressure at the ocean surface and the vapor pressure just above the ocean surface. Increasing the SST will increase the saturation vapor pressure and the latent heat flux will increase as a result. The energy tapped during the evaporation process is subsequently released to the atmosphere through condensation of the water vapor. Latent heat flux is the largest of the various heat transfer processes that occur at the air-sea interface and is expected to dominate the total surface heat flux.

The mean fields of the latent flux (Figs. 16 and 17) show a general trend of increasing flux from the north to the south. This pattern corresponds to the general SST field. The highest fluxes near the western boundary currents are on the order of 15 gm-cal/cm^2-h in the Pacific and 20 gm-cal/cm^2-h in the Atlantic. The effect of the Gulf Stream can be seen more than halfway across the Atlantic and as far as 50°N.

The differences in the latent heat flux for the two model runs show there was an increase in the heat flux into the atmosphere over most of both oceans. The largest increases occurred in the western part of the oceans. Decreases in heat flux (control run compared to the SST run) were associated with decreases in the SST. These decreases occurred in the eastern and southeastern part of the Pacific and in the center and along part of the western boundary of the Atlantic Ocean. The Kuroshio had changes of -3 gm-cal/cm^2-hr over a small region to the east of Japan. The decrease over the Gulf Stream region was as large as -5 gm-cal/cm^2-hr and occurred over a larger area than associated with the Kuroshio.

The standard deviations of the latent heat flux (Figs. 18 and 19) are of the same general pattern and magnitude as the mean field. As for the sensible heat flux, this is most likely due to the effect of the storm passages along the highest SST gradient. There is also a latitudinal dependence resulting from the SST distribution. The diurnal variation of SST may account for the larger values of standard deviation

in the SST run. The resulting variation in the air-sea temperature difference would be larger in the SST run since both the SST and the air temperature vary.

3. Total Surface Heat Flux

The total heat flux is the sum of the latent, sensible, solar (shortwave) and back (longwave) radiation. Latent and sensible heat fluxes have previously been discussed. The total heat flux is expected to have a larger diurnal component than the sensible and latent heat fluxes because of the strong downward component during the day.

The longwave radiation is the heat energy loss by the ocean to the atmosphere or space. The energy is proportional to the fourth power of the temperature (Stefan-Boltzman Law). However, back radiation from the sea surface may be absorbed by clouds or water vapor and reradiated. The effective back radiation is the net longwave radiation loss from the sea surface. Since the SST is relatively constant, the controlling factors are the amount of water vapor in the atmosphere and the cloud amount.

The mean fields of the total heat flux (Figs. 20 and 21) show downward heat flux over most of the ocean. Exceptions are found near the Kuroshio and the Gulf Stream and in a region in the central Atlantic. This region may be an extension of the effect of the Gulf Stream. In these regions, the upward surface heat fluxes exceed the solar flux. The largest magnitudes of 10 gm-cal/cm^2-h occur near the Gulf Stream and the central part of the two oceans.

The regions of downward heat flux are dominated by the solar radiation term which results in a higher SST. The start of the model runs is before sufficient warming of the ocean has occurred for the flux of sensible and latent heat to be large enough to balance the solar heating.

The total heat flux differences between the two model runs are relatively small, which suggests the total heat flux is a result of processes not strongly dependent on the SST. Specifically, at this time of the year, the magnitude of the solar heat flux is beginning to increase, especially in the subtropics and lower mid-latitudes. The atmosphere is almost transparent to the incoming solar radiation and may have a net gain due to the decreased back radiation and sensible and latent heat fluxes at the sea surface.

The standard deviations of the total heat flux (Figs. 22 and 23) show a very large variation about the mean heat flux. This variation is of the same magnitude as the mean fields, with progressive increases toward the south. The largest values of standard deviation are found in the Atlantic Ocean. These large values are due to the diurnal cycle of the solar radiation, as well as the sensible and the latent heat fluxes. The increasing variation from the north to the south is consistent with solar radiation being the dominant factor.

The difference between the two runs also shows the dependence of the total heat flux on the solar radiation. The difference is rather small, and does not appear to have

a strong latitudinal dependence as in the mean field. The time-dependent SST near the western boundary currents contributed to the variation in the sensible and the latent heat fluxes, but did not have as large an effect on the total heat flux. Thus, the mean and variation of the total heat flux are more dependent on the solar radiation than on a time-dependent SST.

C. SUMMARY

Three facets of the air-sea energy transfer have been examined. The sensible, latent and the total heat flux are a function of the SST. The surprising result is the rather small difference between the mean total heat flux for the SST and control model runs. The total heat flux was strongly dependent on the solar radiation, and the changes in SST did not significantly affect the total heat flux. The differences between the two model runs for the sensible and the latent heat flux fields are small, but could be attributed to the SST change. The statistical significance of these changes can not be determined from only one case. The differences of the standard deviations for the sensible and the latent heat fluxes showed the SST run had more variation in the area of the western boundary currents. The differences between the standard deviations of the total heat flux for the control run and the SST run were small. This is consistent with the diurnal variations in the solar radiation being more important in determining the total heat flux than the SST changes. This

result is likely to be seasonally dependent and at different locations the SST variations may become more important in the determination of the total heat flux.

The net change in the energy available to the atmosphere has not been determined. Both the sensible and latent heat fluxes showed general increases with the higher SST in the SST run. This should result in more energy in the atmosphere although the total heat flux values did not appear to change significantly. A question remains on the interrelations among the various heat flux components and the resulting energy available to the atmosphere. Further study into this question, particularly in the tropical regions, will be necessary.

V. CYCLOGENESIS PREDICTIONS

A. INTRODUCTION

The atmospheric response of most importance to an operational forecaster is the forecast of the development and subsequent movement of a cyclone. In a 10-15 day forecast, the model's ability to correctly forecast cyclogenesis would be one of the primary requirements. The two model runs were analyzed as to skill in predicting cyclone development and movement in relation to the actual storm.

An analysis of actual storm developments is thought to be of greater interest than average scores such as root mean square (RMS) height errors or S1 scores. The analysis of cyclogenesis prediction used the Systematic Error Identification System (SEIS) presently under development at the Naval Environmental Prediction Research Facility (NEPRF). SEIS is designed to track individual low storms in either the sea-level pressure or the 500 mb height field. The SEIS program uses the analyzed and the forecast fields to determine various storm parameters, such as the position, the central pressure, the shape and the radius of the storm. These parameters are compared to determine forecast errors. SEIS was modified for this research to intercompare the two model forecasts runs as well as the model run with the analyzed storm parameters. The analysis used the 0000 and 1200 GMT sea-level pressure

fields prepared by FNOC. A more complete description of SEIS can be found in Appendix C.

In addition to the SEIS-derived storm parameters, the average SST and total surface heat flux following the storm center were examined to illustrate the differences caused by changing SST. A simple average over nine grid points centered on the storm was computed at 12 h intervals.

Seven storms were identified by the SEIS program during the 10-day model run. Four of these storms were in the Pacific Ocean and three in the Atlantic Ocean. These storms are identified with a letter for the ocean in which they developed and a number that indicates the sequence in which they developed. For example, storm A1 indicates the first storm developed in the Atlantic Ocean. In the next section, the tracks of the individual storms and the differences in movement of the predicted storms and the analyzed storms are described. The following section summarizes the forecast errors and the differences between the storms forecast by the two model runs.

B. STORM TRACKS

The storms of most significance were the ones that developed late in the forecast period, because these storms will have been exposed to the time-dependent SST for the longest time. Storms P4, A2 and A3 developed over the open ocean after the 90 h forecast time. If the model response, specifically in cyclogenesis, is going to be different as a

result of the time-dependent SST, it should be observed in these three storms. The fact that NOGAPS was able to develop and maintain storms beyond five days forecast time is significant in itself, since such a capability is essential to extend operational atmospheric model runs into the medium-range time period.

Storm P4 developed at 90 h over Asia and continued until the end of the forecast. The SST model run developed this storm 12 h earlier. In all three cases the storm was very weak and extended over considerable distance. The SEIS program had difficulty fitting a regular pattern to this feature which resulted in the large variability in the early storm tracks (Fig. 24). The storm began to organize and develop between 126 h and 138 h when it first crossed from the Asian continent into the Pacific Ocean. After 138 h, the forecast tracks were to the south and lag the actual storm track, which indicated the model was slow in the movement of this storm. The actual storm traveled to the east and stalled at 160°E, 42°N. The forecast storms moved on a northeasterly track and never stalled as in the analysis. The track for the SST run was marginally closer than the control run to the actual track position over the ocean.

The storm parameters (Fig. 25) also show the large variability in the early part of the storm's life and the organizing effect of the ocean surface heat flux at 126 h. The organizing effect resulted in the storm being much better defined,

the SEIS program being able to better fit the storm patterns and the storm tracks becoming more consistent. Starting at 138 h, there is little difference in the SST or the total heat flux for the two model runs. The sizes of forecast storms were considerably smaller than the analyzed storm, but there is little difference between the two forecasts. The central pressures in both forecasts are higher than the actual storm, with the control run being closer to the analysis.

Storm A2 was first processed by SEIS at 102 h (Fig. 26). It began as a small low over the middle Atlantic states and traveled to the northeast. When it crossed into the Gulf of St. Lawrence at 162 h, the additional energy available to the storm from the surface heat flux resulted in a rapid deepening of the storm by 10 mb in 24 h. In both model forecasts this storm developed over the ocean just off of Cape Cod 24 h later. The model storm tracks parallel the actual track, which indicates that after the initial error in the development position, the storms were correctly moved by the model.

The derived storm parameters (Fig. 27) show that this storm was relatively well forecast. There are higher SST early in the SST run but as the storm moves north the SST differences in the two model runs are smaller. The control run has higher heat flux until 174 h when the heat flux becomes larger in the SST run. The central pressure of both model runs is lower than that of the actual storm. The lower

pressure in the forecasts may be due to the additional development since the cyclone was developed over the ocean. The control run forecast is closer to the analysis than the SST run forecast. There is little difference in the storm radius of the two forecasts and both are generally smaller than the actual storm size.

The final storm, A3, developed at 114 h in the middle of the Atlantic Ocean (Fig. 28) and tracked eastward before dying at 186 h. The two model runs handled this storm differently. The SST run forecast deepening 12 h earlier than the actual storm, moved the center to the northeast, and maintained it until 186 h. The control run developed this storm 24 h later and forecast it to remain active until 174 h. The SST run was a better forecast in terms of the forecast development time and life cycle of this storm.

Storm parameters for storm A3 (Fig. 29) show some agreement between the three storms. The SST and heat flux were lower for the SST run. The radius of the storm for both forecasts was larger than that for the analysis. The forecast central pressures were initially too low and the storm began to fill before the actual storm which resulted in higher pressures. The SST run was closer than the control run to the observed behavior over most of the forecast.

The first four storms--A1, P1, P2 and P3--developed earlier in the forecast period than those discussed. The effect of the surface heat flux on the cyclogenesis is

normally minimal compared to dynamical effects during short time periods. Introducing the time-dependent SST into the model should not result in large changes in these storm forecasts.

Storm P1 was present in the Gulf of Alaska at the initial time. The storm track (Fig. 30) was to the southwest before ending at 54 h, while the forecasts terminated the storm at 42 h. The agreement between the two model runs was very good, although both were ahead of the analyzed position. Storm parameters (Fig. 31) also show this agreement. The SST for the control run was lower than the SST run at 30 h. The total heat flux was initially lower for the SST run, but then was almost the same in the two forecasts. The small changes in these inputs resulted in only small changes in the forecast storm. Both the radius and the central pressure were not changed. As expected, early in the model run the time-dependent SST did not cause a change in the model response.

During this early period, the Atlantic Ocean was dominated by the subtropical high and no storms were in this area. Two storms, A1 and P2, developed after the 66 h into the forecast. At the time SEIS began to track Storm P2, it was already in a mature stage and began to occlude and fill. Storm P2 was followed until 126 h (Fig. 32). During this time it was almost stationary in the Bering Sea. The storm centers in the two model runs were to the southeast of its observed location. The track for the control run began to turn to the

southeast while the track for the SST run moved into the vicinity of the actual storm. The storm parameters (Fig. 33) further indicate the SST run provided a marginally better forecast for this storm. The SST run continued the storm to the same time as the analysis, whereas the control run ended the storm 24 h early. The storm radius for the SST run was also closer to the analyzed size. However, the error in central pressure for the SST run was greater than for the control run. The storm center in the control run remained farther to the south over warmer water. The total heat flux at the storm center in the control run was larger, which is consistent with the lower central pressure.

As storm A1 developed over Scandinavia (Fig. 34), the time-dependent SST should not have a large effect on the cyclogenesis. The storm traveled to the northeast, while the two model run tracks were toward the south. The storm parameters (Fig. 35) show the SST run had less error. The storm in the SST run remained active for as long as the analyzed storm. The radius for the SST run was also closer to the actual storm radius. The magnitude of the central pressure error was about the same, although it was too low in the control run and too high in the SST run. This is most likely due to the storm in the control run being located over the Baltic Sea, while the storm in the SST run was over land. The surface temperature and heat flux reflect this difference in location.

The next storm that developed was storm P3 (Fig. 37) at 90 h of the forecast. This storm in the Gulf of Alaska moved to the north across Alaska. The two forecast storm tracks seem close to this path, but with very different timing (Fig. 38). The control run forecast storm development 24 h early and dissipation 12 h after the storm actually started. The SST run began the storm at the same time as the analysis but had predicted the end of the storm 36 h too soon. Comparisons of central pressures, storm radius, SST and heat flux (Fig. 38) are difficult due to the different periods these storms were active. In general, the forecast central pressure was too high, with the SST run having greater errors than the control run. The SST for the control run was higher and the heat flux was higher in the early stages of the storm, which would account for the lower central pressure.

C. FORECAST DIFFERENCES

The forecast position, intensity and movement of a cyclone are among the most important parameters an operational meteorologist can use to determine future weather conditions for an area. These parameters were objectively determined by the SEIS program for each period a storm was active. Differences in these parameters were then summarized to determine changes in the cyclogenesis as forecast by the two model runs. Position differences are described in terms of latitude and longitude and the total distance between two positions. The

latitude and longitude difference can also be used to determine if there is a consistent error in the forecast movement of a storm. Storm intensity was determined from the central pressure and the radius of the storm.

A summary of the differences between the two model runs and the analysis and each of the two model runs is given in Table 1. Means and standard deviations for each parameter of each storm were computed. It should be noted that the largest number of forecast times (12 h intervals) is only eleven. Thus it is difficult to determine the statistical significance of the average difference values.

The forecast central pressures were generally higher than those for the analysis. The exceptions were early in the forecast for storms P1, A1 and for storm A3 which developed over land. Both the control run and the SST run underforecast the central pressure relative to the analysis, but the error was smaller for the control run than for the SST run. The central pressures of storms A1 and A3 are better forecast by the SST run. Recall that storm A3 was poorly forecast by the control run. Storm A2 was better forecast by the control run. This storm developed over land while the model placed it over the ocean.

The radius differences of the storm vary widely and have large standard deviations. In almost all cases, the storm radius forecast in the SST run was closer to the analysis than was the control run.

The latitude differences indicate the SST run consistently placed the storm farther to the north than the control run. This may be due to the warming of the sea surface due to the time-dependent SST. The longitude error shows storms in the SST run were generally to the east of the storms in the control run. The combined latitude and longitude differences indicate that the storms in the SST run had moved faster than in the control run. Distance differences in the position of the storm for the two runs vary. The most important result is for storm P4. This storm had a small distance difference even though it had a long life cycle and was present in the later stages of the forecast. Storms A2 and A3 also had small differences in position. When the two model run positions are compared with the analysis, the positions from the control run forecasts are better. However, it is difficult to determine the significance of this result due to the large standard deviations.

D. SUMMARY

Seven storms were identified during the 10-day forecast period and objectively analyzed using SEIS. Storms A1 and P1 appeared in the early forecast period before the effect of the time-dependent SST was large. Storm P3 was generally over Alaska and the effect of a time-dependent SST was also small. The remaining storms P2, P4, A2 and A3 were the storms most affected by the time-dependent SST, although the changes are not very large. In general, the central pressure

forecast by the control run was closer to the analysis than was the SST run forecast. The positions of the storm for the control run were also closer to the analyzed position.

The biggest improvement in the SST run was that the life of the storm was closer to the actual life of the storm. This change was most apparent for storm A2, but could be seen for other storms, particularly A1 and P2.

TABLE 1

Difference in storm parameters. SST indicates SST run. Con or Cont indicates control run. Anal indicates values from the analysis. The first number in each column is the mean and the second is the standard deviation. Start and end times are for the analysis

CASE	Items	P (mb)	Radius (km)	LAT	LONG	Dist (km)
		Storm: A1	Start: 66h	End: 138h		
SST-Cont	4	3.7/0.9	-22.6/302.8	2.1/2.6	3.4/6.9	227.3/178.2
Con-Anal	3	-2.4/1.8	-24.7/302.7	-4.0/0.8	-8.3/8.7	306.3/241.1
SST-Anal	7	-0.6/2.5	-33.0/143.8	-3.8/3.1	7.3/13.7	421.8/212.1
		Storm: A2	Start: 126h	End: 186h		
SST-Cont	4	-4.2/1.5	22.6/127.8	1.5/1.0	-0.5/0.3	94.7/60.6
Con-Anal	4	1.7/4.8	354.6/266.8	4.5/0.6	6.7/4.0	398.8/101.7
SST-Anal	6	0.6/4.1	311.5/196.2	5.1/1.9	3.9/4.9	371.1/148.6
		Storm: A3	Start: 126h	End: 234h		
SST-Cont	10	-1.7/2.5	36.4/133.0	-1.2/0.9	-0.2/3.2	117.5/82.9
Con-Anal	10	-7.8/3.8	-203.1/227.1	-5.5/2.4	-10.7/4.0	512.9/133.9
SST-Anal	10	-9.5/3.5	-112.5/234.2	-6.7/2.8	-10.9/6.1	559.8/208.9
		Storm: P1	Start: 6h	End: 42h		
SST-Cont	4	-0.1/0.2	-16.1/32.3	-0.1/0.	-0.1/0.3	19.1/0.4
Con-Anal	4	-1.6/1.8	57.6/85.1	-0.1/1.	-0.8/1.3	69.6/46.1
SST-Anal	4	-1.7/1.8	41.5/106.1	-0.2/1.1	-0.9/1.4	74.9/55.3
		Storm: P2	Start: 66h	End: 162h		
SST-Cont	6	1.7/3.0	171.2/228.9	1.8/2.9	-1.9/3.4	142.6/202.2
Con-Anal	3	7.9/3.4	-197.9/186.0	-4.5/3.8	4.2/6.8	404.8/115.9
SST-Anal	4	9.4/1.8	-7.5/175.3	-2.7/2.9	-6.9/6.2	379.4/87.3

TABLE 1 (Cont.)

CASE	Items	P (mb)	Radius (km)	LAT	LONG	Dist (km)
		Storm: P3	Start: 90h	End: 162h		
SST-Cont	3	2.9/2.4	-21.8/102.7	3.3/4.5	-0.9/4.8	214.3/273.2
Con-Anal	3	2.5/2.2	179.8/409.3	6.9/0.9	3.6/16.5	584.4/66.6
SST-Anal	7	5.7/2.9	69.0/347.5	8.6/5.4	-0.5/13.3	625.7/285.5
		Storm: P4	Start: 90h	End: 234h		
SST-Cont	10	1.1/1.7	134.1/60.8	0.5/0.7	0.5/1.0	69.7/26.9
Con-Anal	11	1.4/1.5	-314.7/400.5	-0.4/5.6	-1.0/4.9	352.9/148.1
SST-Anal	11	3.3/2.6	-277.3/280.7	1.2/6.	-6.0/12.6	517.6/371.5

VI. CONCLUSIONS

The goal of this research was to determine the response of an atmospheric forecast model to a time-dependent sea surface temperature (SST). The results were surprising in that there was little change between the two model runs. Specifically, the following conclusions were reached:

(1) The total heat flux was strongly dependent on the solar radiation. This was indicated by the small differences between the mean total heat flux for the two model runs and the large standard deviations.

(2) The differences in the latent and the sensible heat fluxes were also small but could be attributed to the change in SST.

(3) NOGAPS has the ability to generate and maintain a cyclone beyond five days forecast time. This is an important ability for a numerical model to possess before the forecast period can be extended into the 10-15 day range.

(4) Differences between the SST run and the control run were small compared to the standard deviation of the changes. Thus, the statistical significance and any improvement in forecast skill cannot be determined with confidence.

(5) In general, the control run forecast central pressure and position of storms was better than the SST run. The life cycles of individual storms were better forecast by the SST run.

This study was limited in its application and results. The initial conditions were chosen to be able to determine the changes in the atmospheric model during the spring transition in the ocean. A decrease in the SST was expected in the wake of a cyclone which would have decreased the amount of cyclogenesis in the SST run. However, a general increase

in SST was observed and this hypothesis could not be tested. Additionally, SST fields were only available for the first 7.25 days of the model run. This may have reduced the size of the differences between the two model runs.

It is recognized that one case study is not a statistically significant sample. Additional case studies following the same approach need to be conducted before the full impact of a time-dependent SST on an atmospheric model can be determined. These studies should be expanded to include the following: (1) A model with higher vertical resolution should be used. Specifically, the nine-level version of NOGAPS which is now available will serve to improve the propagation of the effects of the changing surface heat fluxes into the atmosphere. (2) The analysis should be extended to include additional model variables and geographical areas. Cloud patterns, precipitation and other diabatic effects need to be examined to determine their impact on the model response. Additionally, model changes in the equatorial and tropical regions will need to be examined. (3) The role of fluxes across the air-sea interface requires additional study with the goal of improving the parameterization of the fluxes. It is felt that the small changes in fluxes in this study resulted in part from limitations in the parameterization method.

APPENDIX A

THE NAVY OPERATIONAL GLOBAL ATMOSPHERIC PREDICTION SYSTEM

The Navy Operational Global Atmospheric Prediction System (NOGAPS) used at the Fleet Numerical Oceanography Center (FNOC) is a slightly modified version of the UCLA general circulation model. NOGAPS has been the Navy's operational atmospheric forecast model since August 1982. The following sections describe the various features of NOGAPS as used during the experiment. The complete model has been described by Rosmond (1981).

A. DYNAMICS

The dynamics of the UCLA GCM are described in detail by Arakawa and Lamb (1977) and are only discussed briefly here. NOGAPS is a primitive equation model. The prognostic variables are horizontal velocity, V, temperature, T, surface pressure, p_s, and specific humidity, q. Additional prognostic variables associated with the planetary boundary layer (PBL) will be described below. The finite difference scheme used has a spatial resolution of 2.4° lat by 3.0° long. The variables are staggered in the horizontal according to Arakawa scheme C (Fig. 38). The center grid point contains the T value. The meridional wind component, v, is carried at points north and south of the center point andthe zonal wind component, u, is carried at points east and west of the center

point. The numerical differencing scheme is both energy and enstrophy conserving.

NOGAPS uses a sigma coordinate system in the vertical defined as:

$$\sigma = (p - p_i)/\pi$$

where:

$$p_i = 50 \text{ mb} \quad \text{and} \quad \pi = p_s - p_i ,$$

p is pressure and p_s is surface pressure. There are six model layers in the vertical with the top of the model atmosphere at 50 mb. All prognostic variables except vertical velocity, $\dot{\sigma}$, are carried at the middle of each layer. Vertical velocity is carried at the layer interfaces (Fig. 39).

NOGAPS uses a second order (leapfrog) time difference scheme with a four minute time step. Model diabatics are executed every forty minutes. A Matsuno time step is used every fifth time step. This is used to control the computational mode and to assist in the assimilation of the diabatic effects. In regions above 60° latitude, a special Fourier filter is used to avoid an extremely short time step. Whereas a simple three point filter is used equatorward of 60 deg. This filtering reduces the amplitudes of the zonal mass flux and pressure gradients and maintains computational stability.

B. MODEL DIABATICS

The sophisticated model diabatics contained in NOGAPS is an important component in this experiment. This treatment of the diabatic processes is necessary to adequately simulate fluxes across the air-sea interface and to propagate the full effect of these changes throughout the atmosphere. NOGAPS directly computes the physical processes for:

dry convective adjustment
large scale precipitation
diagnosis of stratus cloud depth
mid-level convection
ground hydrology
surface friction
horizontal diffusion of momentum
radiative transfer processes
cumulus convection

1. Planetary Boundary Layer

The planetary boundary layer (PBL) is defined as a well mixed layer in moisture, moist static energy and momentum. It is assumed to be capped by discontinuities in temperature, moisture and momentum. The PBL treatment in this model follows Deardorff (1972) and has been formulated for the UCLA GCM by Randall (1976). It allows for interaction between the PBL and cumulus cloud ensembles and/or a stratus cloud layer at each grid point. Surface fluxes are determined using a bulk Richardson number based on the values of the sea surface temperature and the values of V, T and q from the adiabatic portion of the model. These values are then used to predict a new PBL depth and thre strength of the inversion jumps.

The NOGAPS PBL is constrained to remain in the bottom sigma level of the model. This differs from the original formulation of the UCLA GCM, in which the PBL was allowed to pass out of this layer. An overly deep PBL can result in serious computational problems with the model. Constraining the PBL this way imposes a maximum depth of about 200 mb on the PBL.

2. Cumulus Parameterization

Cumulus parameterization in NOGAPS follows the scheme of Arakawa-Schubert (1974) as introduced into the model by Lord (1978). In the model, cumulus clouds must have their bases at the top of the PBL. Cloud tops can be at all sigma levels above the PBL. Cumulus clouds are modeled as entraining plumes in which environmental air is mixed with the PBL air from which the cloud originated. Tendencies of moisture, temperature and momentum are diagnosed as well as the cloud mass flux. The cloud base mass flux removes mass from the PBL, which decreases the PBL depth. Condensation occurs at each grid point where the air becomes supersaturated. A moist convective adjustment procedure removes convective instability between mid-tropospheric layers that is not eliminated by clouds originating from the PBL.

3. Radiation

The radiation parameterization follows Katayama (1972) and Schlesinger (1976). It includes both a diurnal variation and interaction with the cloud distribution. Radiative

transfer processes for incoming solar radiation are computed. Effects of water vapor, Rayleigh scattering by air molecules and absorption and scattering by water droplets in clouds are included. Reflection due to clouds is also calculated. The model cloud cover predicted by the PBL, the cumulus parameterization and large scale precipitation interact with the long wave radiation. The net surface heat flux is computed as a function of the incoming solar heat flux, long wave radiation and sensible heat flux. In the present model, this affects only the surface temperature over bare land and ice and has no effect on sea-surface temperature.

APPENDIX B

THERMAL OCEAN PREDICTION SYSTEM-EXPANDED OCEAN THERMAL STRUCTURE (TOPS-EOTS)

The Navy began using the TOPS-EOTS system as the operational ocean thermal analysis and forecast system in March 1983. The objective analysis component is a modified version of the conventional EOTS analysis for the northern hemisphere. The forecast component, TOPS, is a synoptic mixed layer model.

The Expanded Ocean Thermal Structure (EOTS) [Mendenhall, et al., 1978; Holl, et al., 1979] has been the Navy's operational ocean thermal analysis system for the past several years. It is used to objectively analyze the approximately 200 XBT and 2000 surface ship observations reported to FNOC in real time each day [Clancy, 1981]. With some modification, the conventional EOTS analysis has become the objective analysis component of TOPS-EOTS. The analysis is performed on the FNOC 63 x 63 hemispheric polar stereographic grid. The EOTS analysis is performed for the Northern Hemisphere only. Due to the small number of available subsurface temperature profiles, a sea-surface temperature analysis only is performed in the Southern Hemisphere.

The EOTS analysis is carried out using a Fields by Information Blending (FIB) methodology [Holl and Mendenhall, 1971]. This falls into the broad category of objective analysis

known as successive corrections. Twenty-six ocean parameters are analyzed in the upper 400 m on the vertical grid shown in Fig. 40. Parameter one is the primary layer depth (PLD), which is approximately the depth of the seasonal thermocline. The remaining parameters are temperatures and vertical temperature derivatives. Parameters 2-8 are analyzed at floating levels defined relative to the PLD and parameters 9-26 are associated with fixed levels.

The first guess field is the previous 24 hour TOPS forecast. The first guess field is horizontally blended, with the observations available for each of the eighteen fixed levels parameters. The analysis is performed over a three-cycle assimilation using reevaluated weights at each grid point during each cycle. The floating parameters are analyzed in the same manner, but with the added complication of determining the PBL. Next, a vertical blending process is performed. Vertical blending minimizes inconsistencies in the vertical in a weighted least squares sense. This is completed in one step as opposed to the three-cycle analysis used in the horizontal blending. The sea surface temperature is given an extremely high weight, which effectively anchors the upper part of the thermal profile to this field.

The forecast component, which is designated as the Thermal Ocean Prediction System (TOPS) [Clancy and Martin, 1979; Clancy, et al., 1981], is a synoptic mixed layer model that employs the Mellor and Yamada (1974) Level-2 turbulence

parameterization scheme. It includes advection by instantaneous wind drift and climatological geostrophic currents. The horizontal grid used is the FNOC 63 x 63 Northern Hemisphere polar stereographic grid. The values of the mean temperature, T, mean salinity, S, and mean north-south and east-west currents, v and u, are carried at each grid point. Additionally, the advection currents u_a and v_a are carried at grid points displaced one-half grid length in the x- and y-directions. The vertical grid includes 18 levels between the surface and 500 m. The variables T, S, u, v, u_a and v_a are carried at each level. The vertical eddy fluxes and vertical advection velocity, w_a, are carried at the mid-levels.

The initial conditions for the temperature fields are provided from the EOTS analyses. An initialization algorithm is used to match the EOTS analysis to the vertical levels used in TOPS. Salinity is determined by interpolation of monthly climatology. Wind velocity, surface heat flux (sensible heat, infrared radiation and latent heat) are provided from NOGAPS every six hours and are linearly interpolated to each time step of the model run.

APPENDIX C

THE SYSTEMATIC ERROR IDENTIFICATION SYSTEM (SEIS)

SEIS is a tool to objectively analyze numerical model predictions and produce error statistics for use by operational forecasters. It is presently being implemented for operational use with NOGAPS by the Navy Environmental Prediction Research Facility (NEPRF). The system has been described by Harr et al., (1982). SEIS operates in a quasi-Lagrangian frame with the reference center located at the center of the storm.

The primary algorithm within SEIS is the vortex tracking program (VTP) after Williamson (1981). The purpose of VTP is to track synoptic-scale features and produce a listing of operationally relevant parameters following the feature. This program allows each vortex to be examined individually and followed in time. The parameters chosen include amplitude (A), ellipticity (ε), radius (R), orientation (α), and position of the feature. Amplitude is the magnitude of the vortex central pressure relative to the zonal mean pressure. Ellipticity is a measure of the deviation of the shape of the storm from circular. It is computed as the square of the ratio of the semi-major and semi-minor axes. Orientation is the angle between the x-axis and the semi-major axis, measured counterclockwise from the positive x-axis. Position is

specified as either the model grid position or the geographical position.

The first step in the VTP is to extract the atmospheric low pressure systems from the sea level pressure fields. After removing the zonal mean pressure, a series of ellipses is fit to the vortices to determine if the low pressure systems are generating, dying, merging or splitting. The original SLP field has now been reduced to a set of parameters describing the ellipses which define the low pressure systems in terms of A, R, ε, α and position. Each low pressure system is assigned a unique name.

After all maps during a forecast interval have been completed, the fitted parameters are transformed to raw verification data and raw error statistics. The raw error statistics are differences between the forecast and verifying analysis values of a system's parameters, A, R, ε, α and position. Additional derived errors are produced as shown in Fig. 41. Forecast error is the distance between forecast and verifying positions. Track error is the shortest distance between the forecast position and the track position. Timing error is the hourly difference between the verifying position and the position on the verifying track closest to the forecast position. Speed error is the difference between the distance traveled by the forecast and verifying centers divided by the time increment. Heading error is the angle between the forecast and verifying positions measured from the analysis position.

Some modifications were made to SEIS for the purposes of this study. The VTP analysis was extended from the normal 48 h period to 10 days for the longer model forecasts produced in this study. Storms generated during this period required special fitting with the analysis. Also, SEIS was originally designed to compare the forecast field with a verifying field. It was adapted to compare either of the two model runs to the analyzed fields, or one model run to a second run, or all three possibilities at the same time.

APPENDIX D

FIGURES

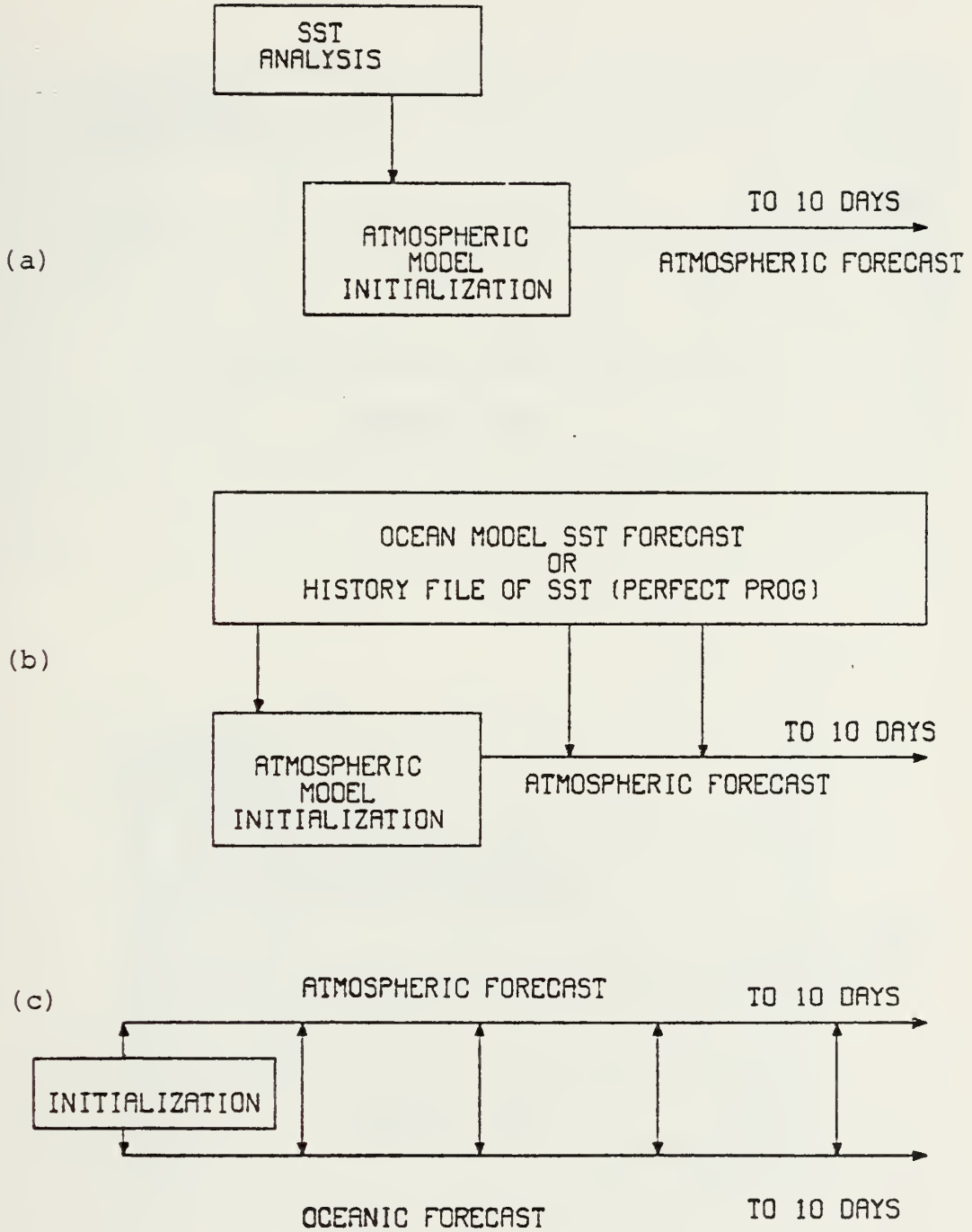

Figure 1. Methods for coupling atmospheric and oceanic models (a) minimal feedback, (b) non-synchronous and (c) synchronous.

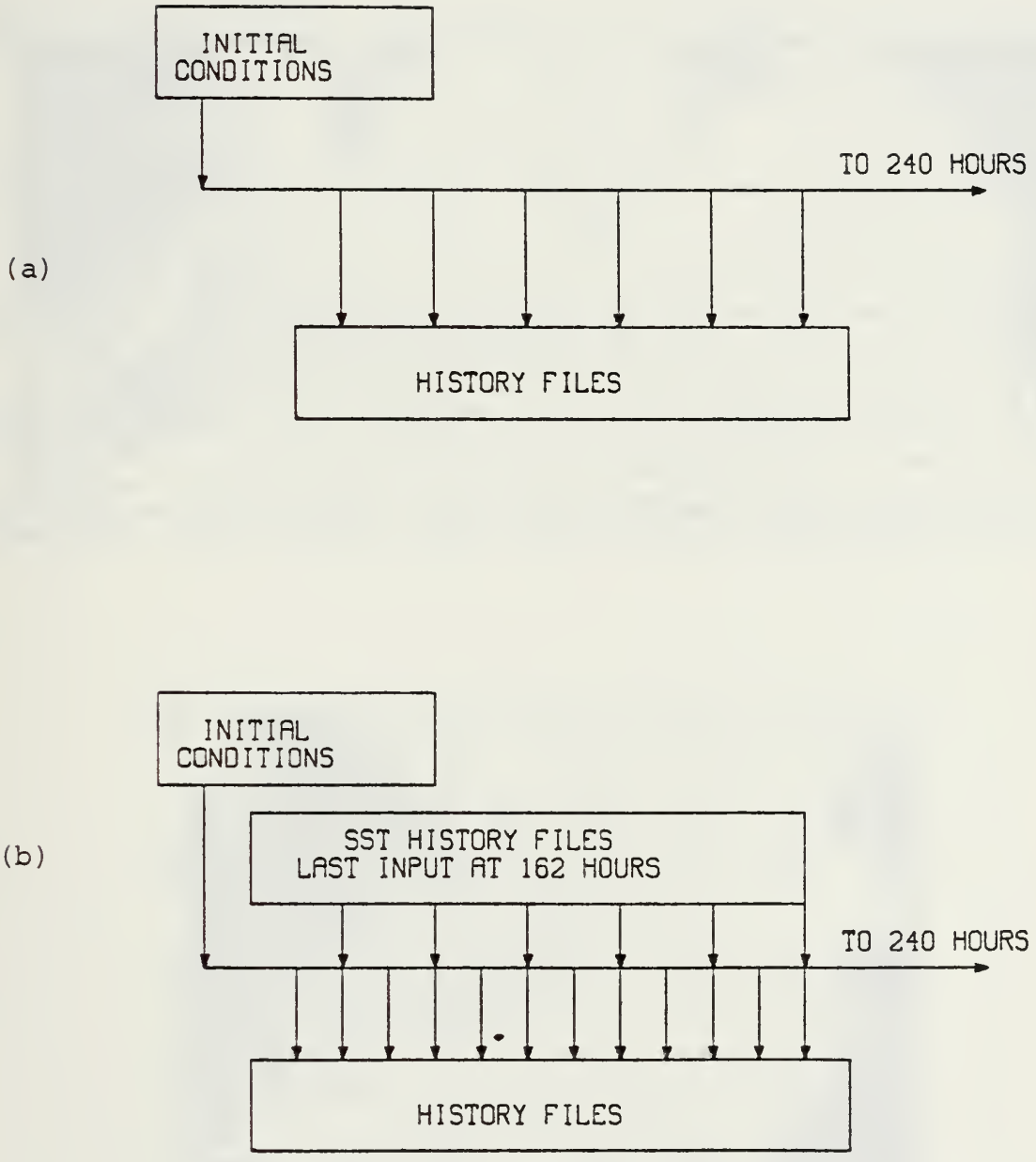

Figure 2. Schematic of experiment design for (a) control run (b) SST run. SST fields input every twelve hours. History files output every six hours.

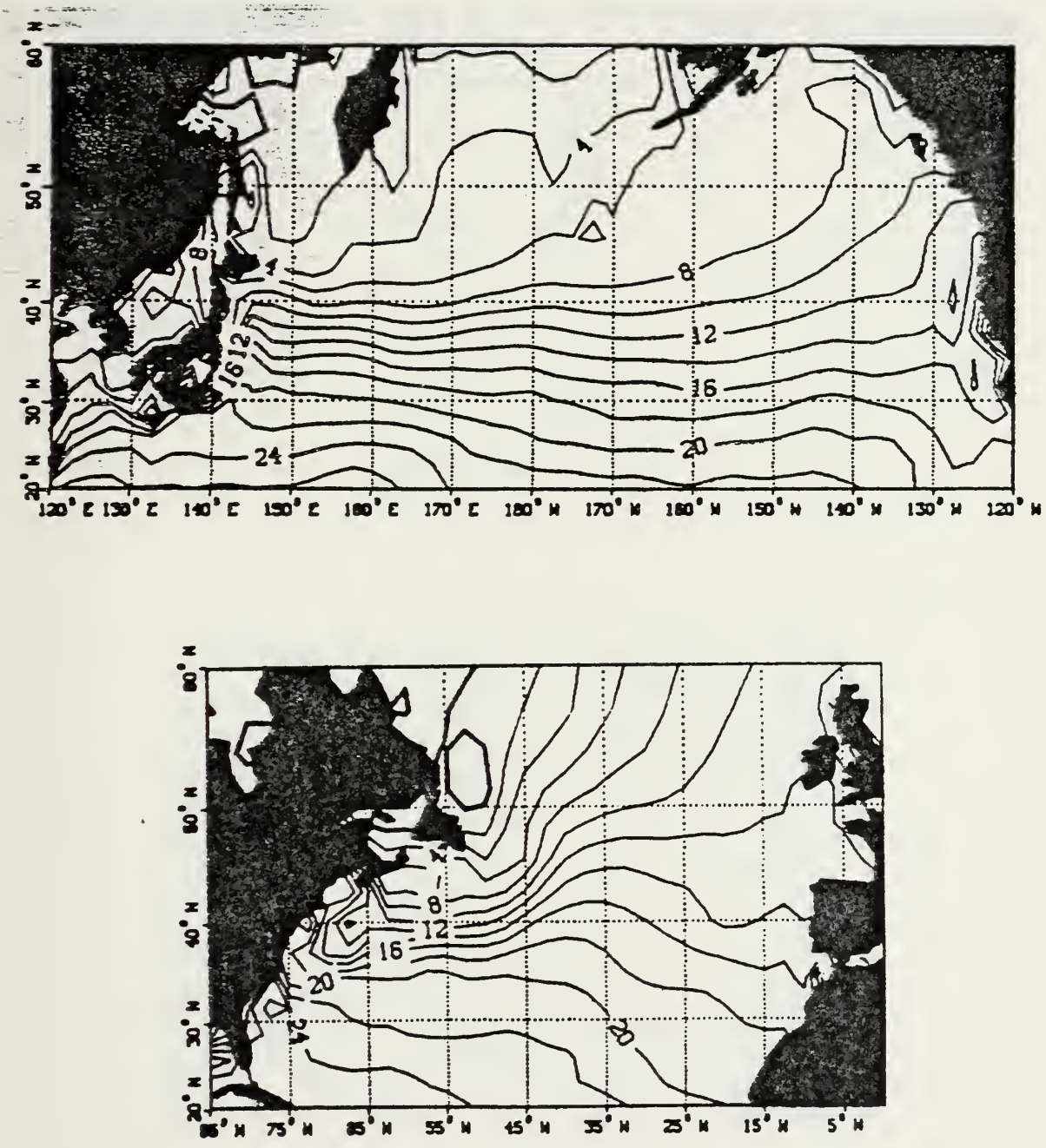

Figure 3. Sea surface-temperature fields used in the initial conditions in the model run. Contour interval is 2°C.

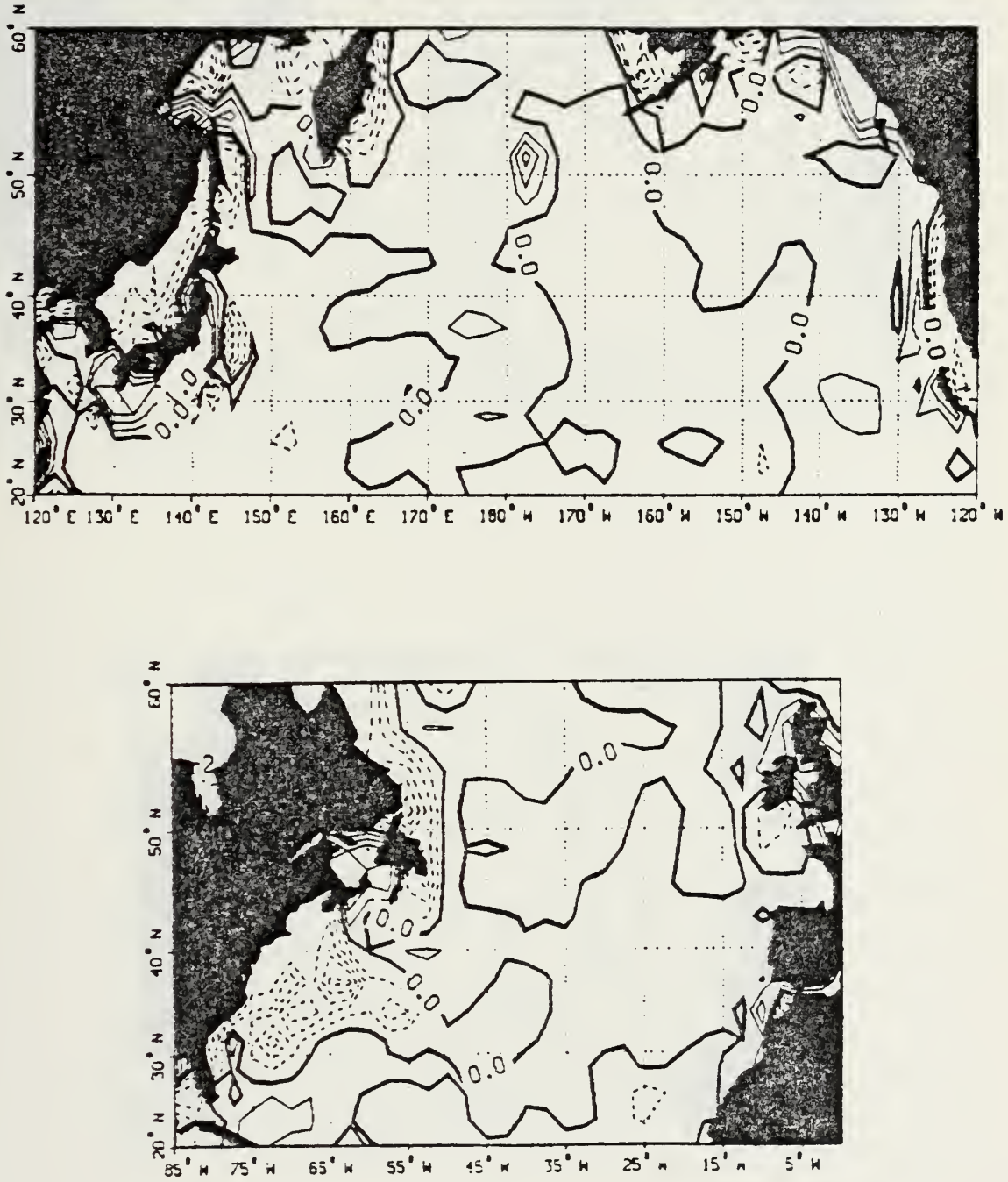

Figure 4. The difference between the SST field input at six hours of the model run and the initial SST field. Contour interval is 0.5°C. Thin solid lines are higher SST, thick solid is no change and the dashed lines are lower temperature.

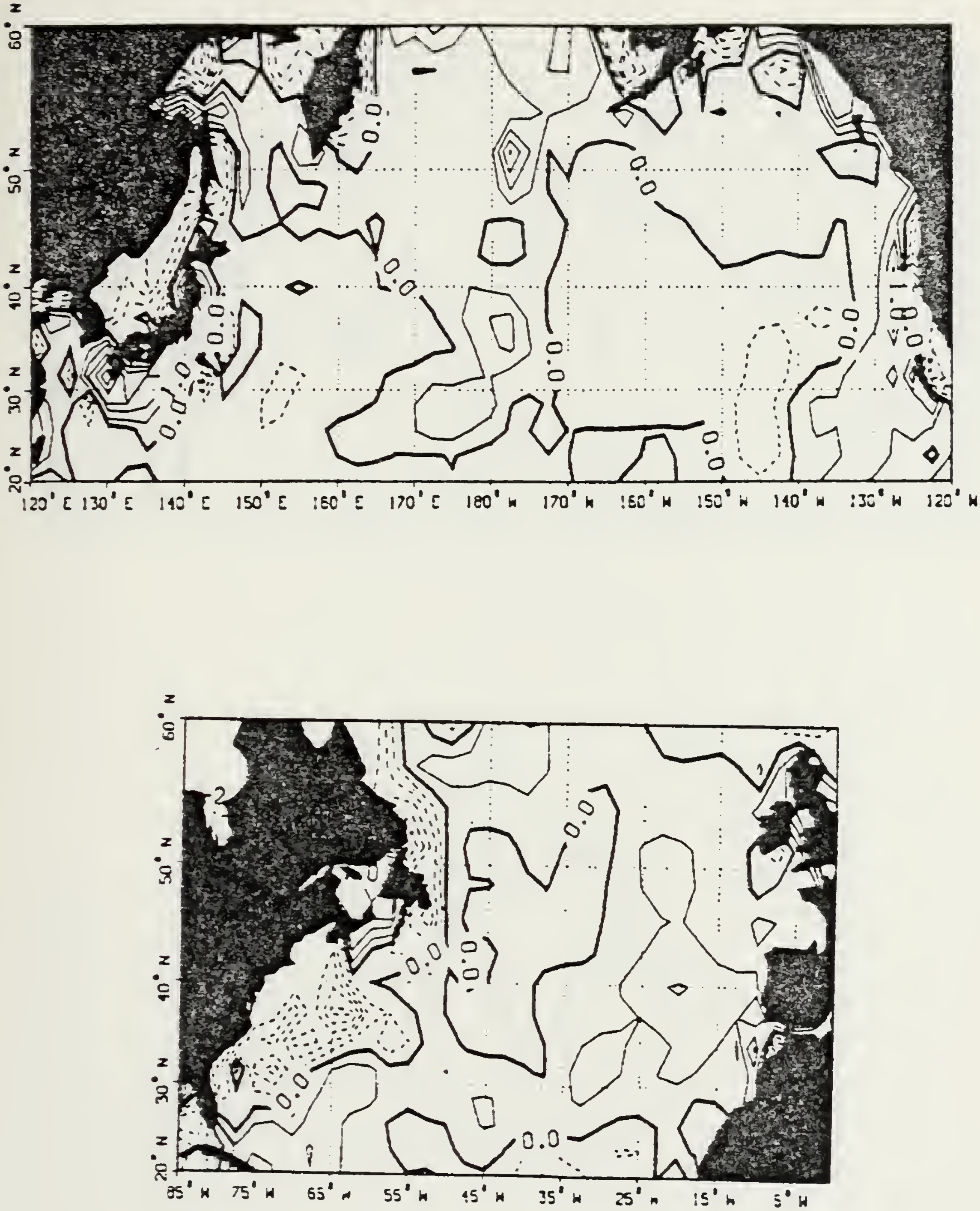

Figure 5. As in Fig. 4, except for 30 h.

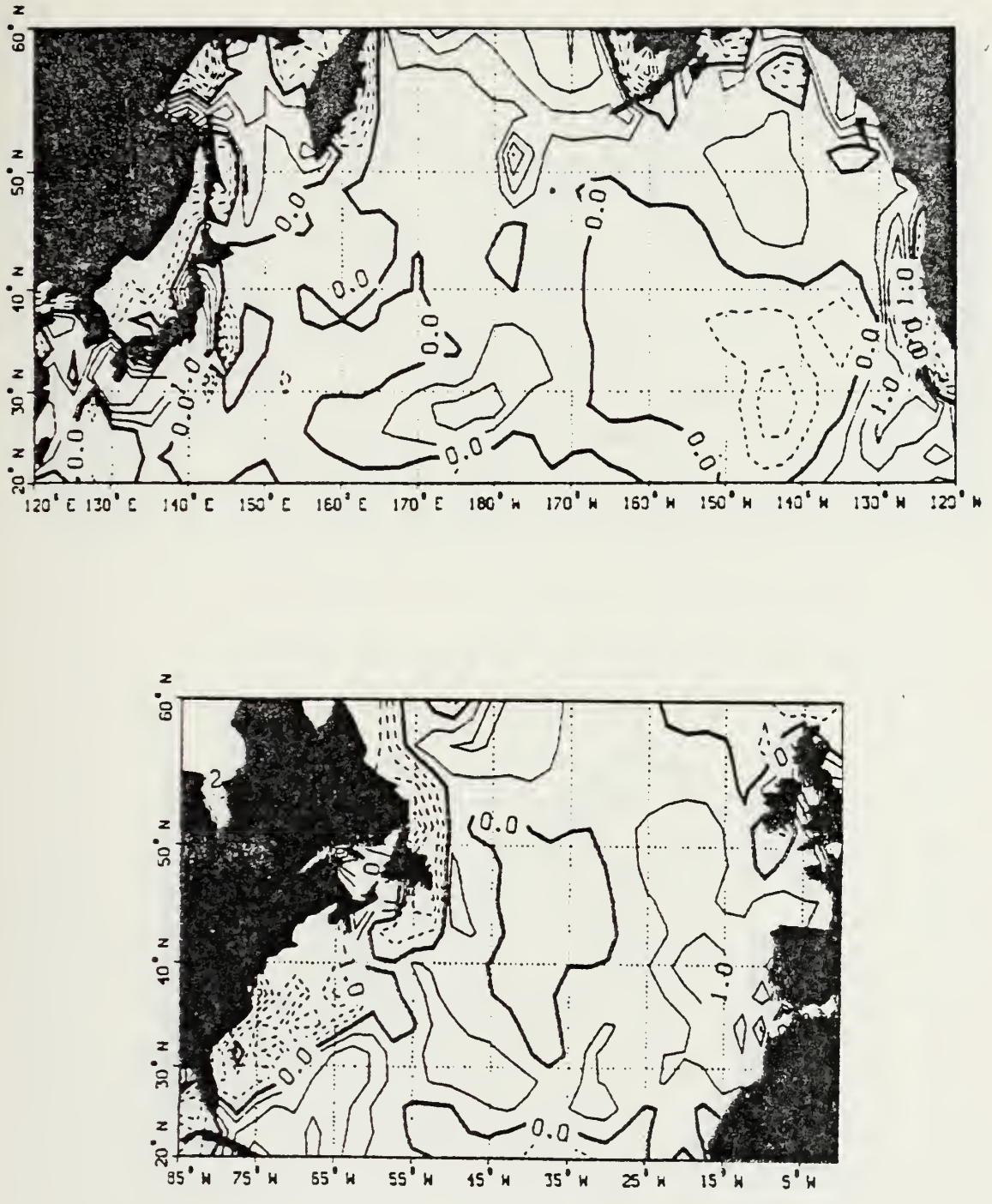

Figure 6. As in Fig. 4, except for 54 h.

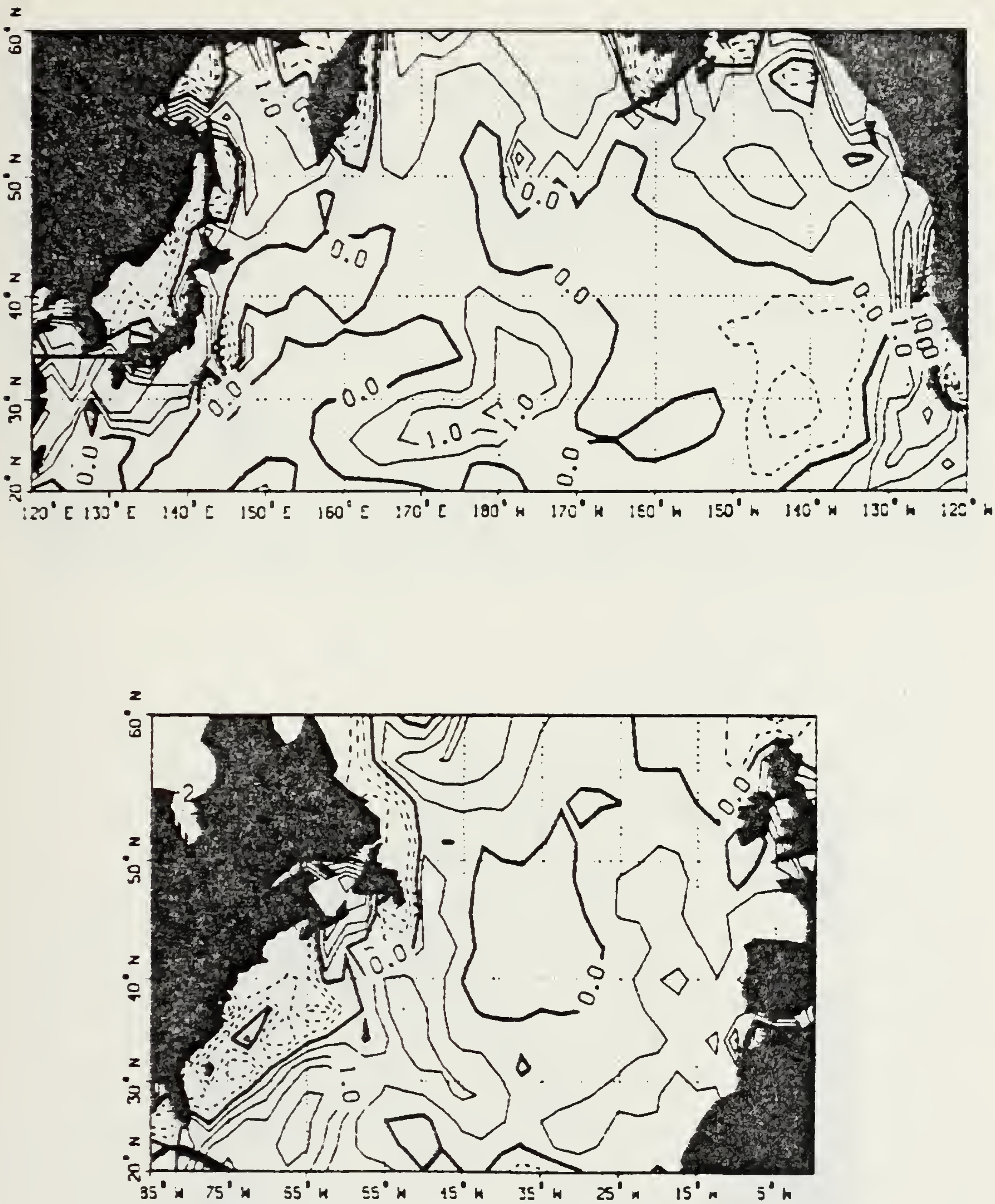

Figure 7. As in Fig. 4, except for 78 h.

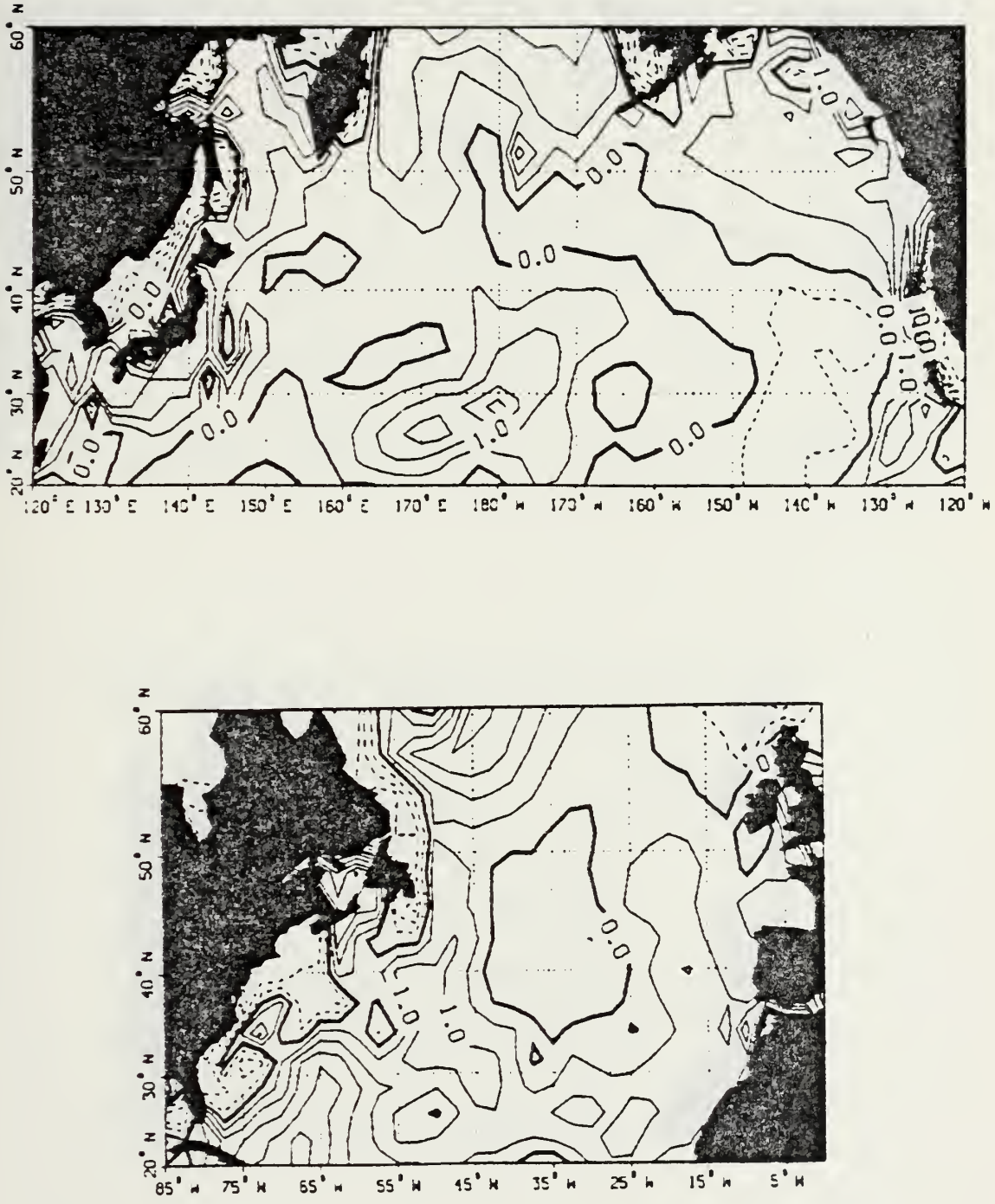

Figure 8. As in Fig. 4, except for 102 h.

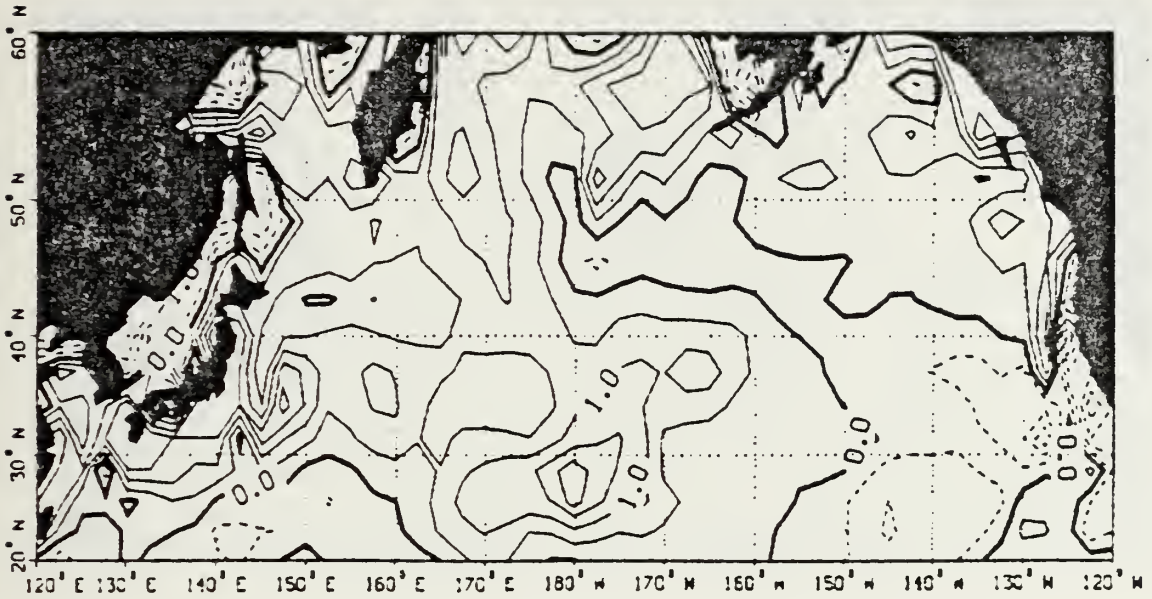

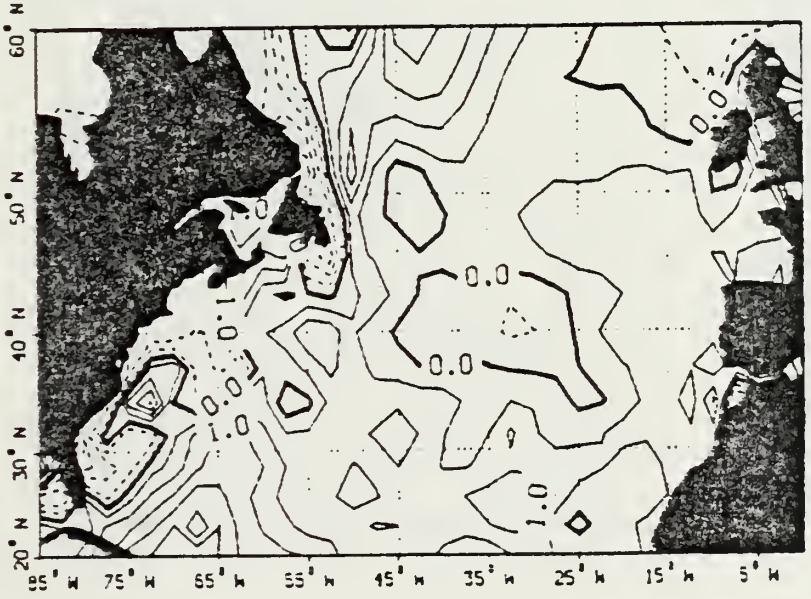

Figure 9. As in Fig. 4, except for 126 h.

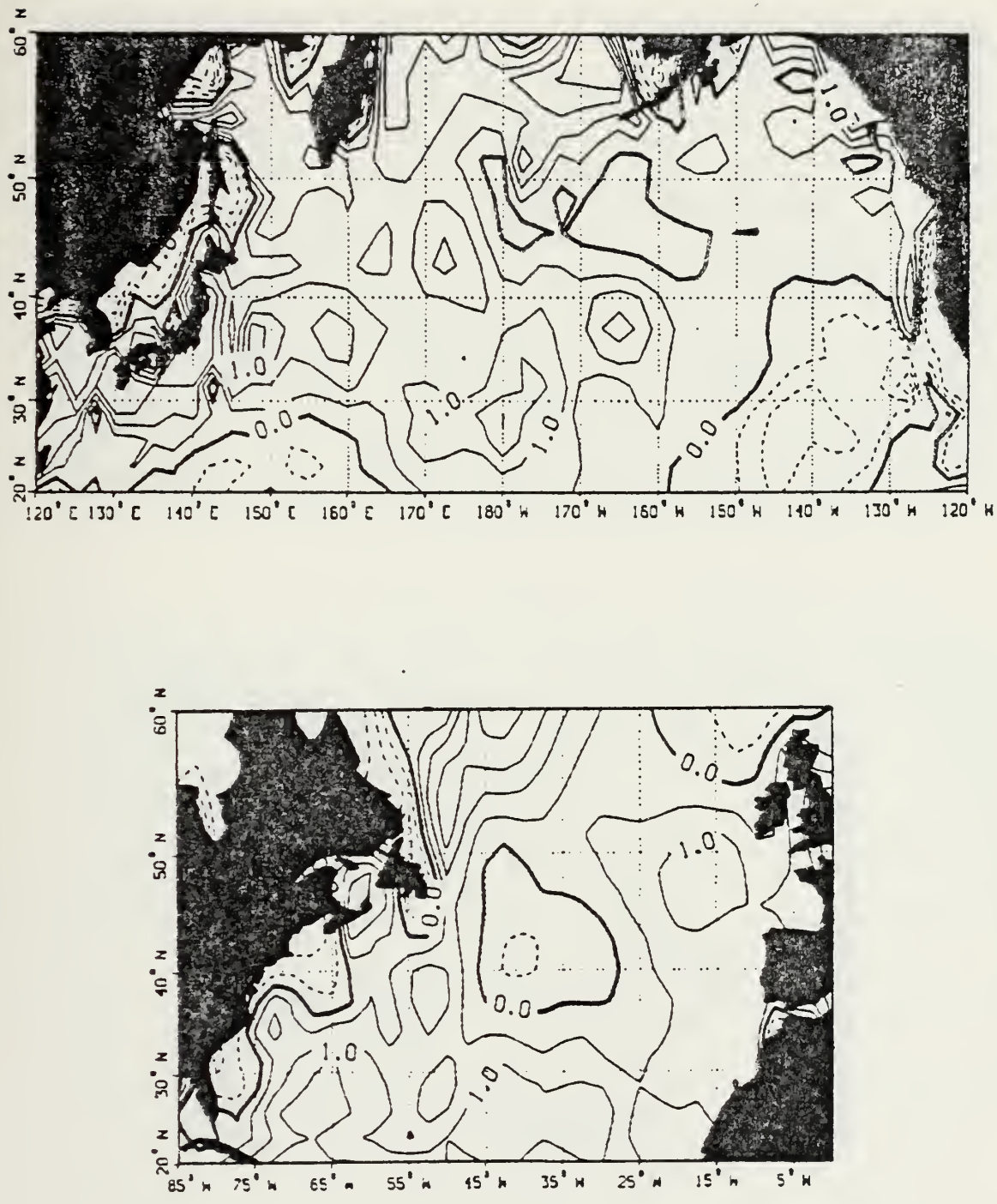

Fig. 10. As in Fig. 4, except for 150 h.

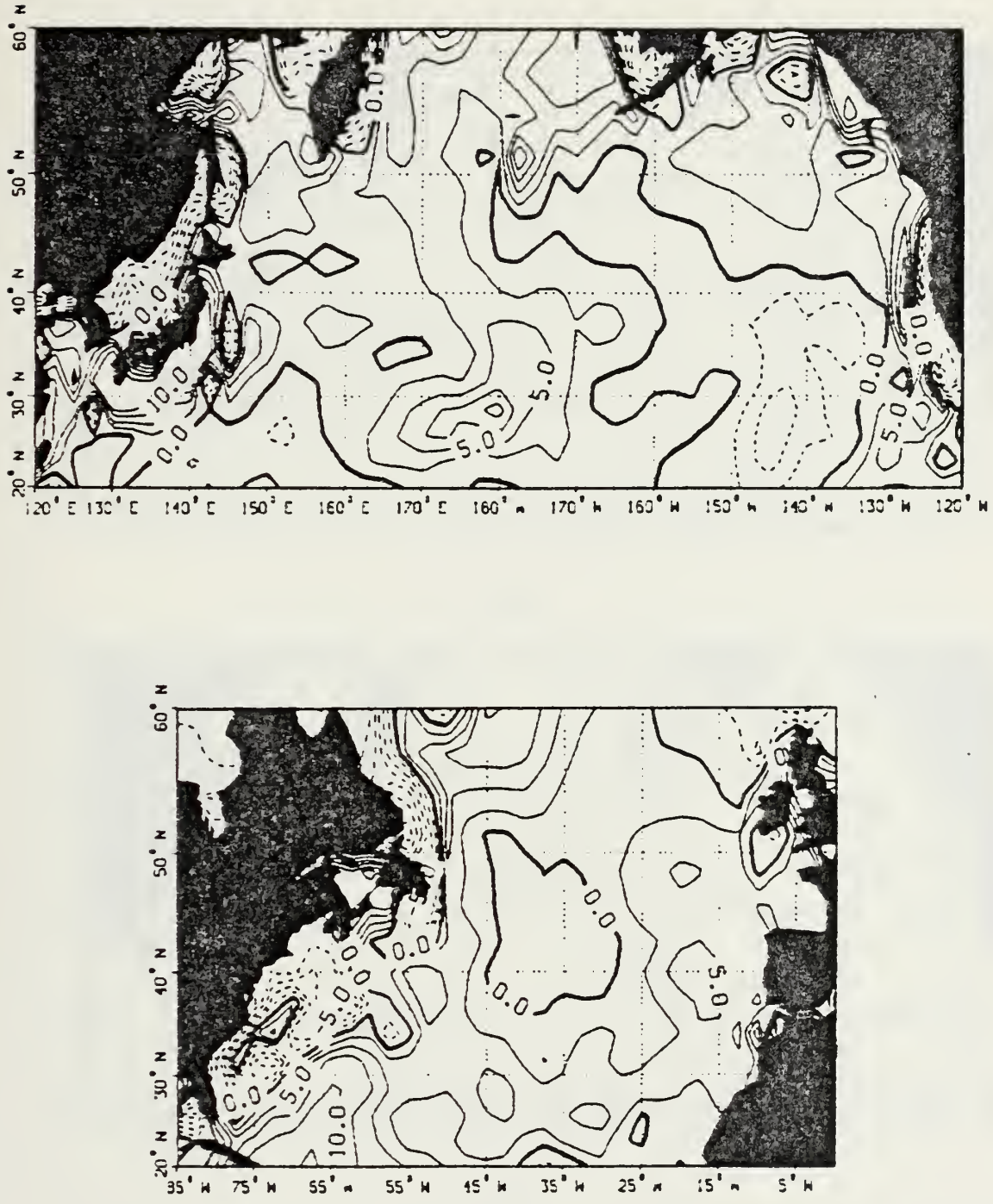

Figure 11. The cumulative change in the SST field summed over 24-h intervals. Contour interval is 2.0°C.

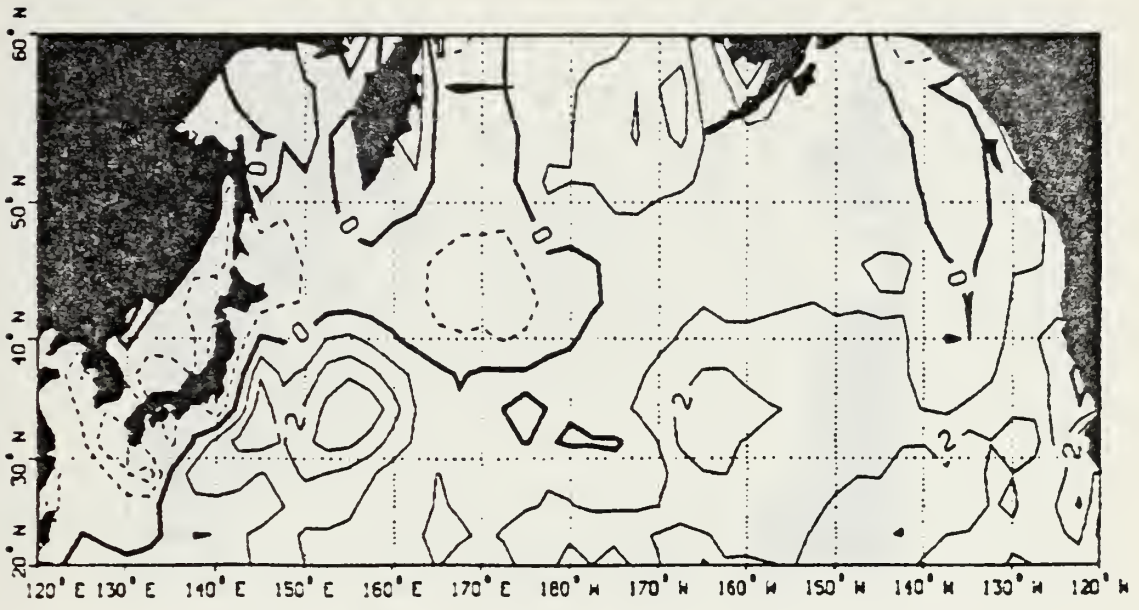

(a)

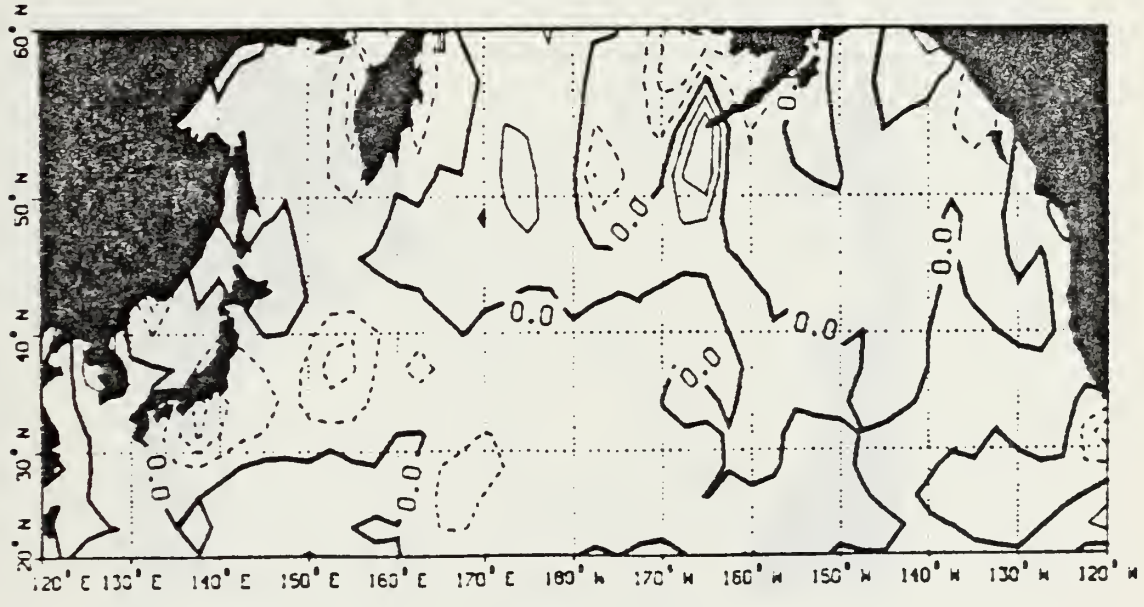

(b)

Figure 12. (a) Mean sensible heat flux for the Pacific Ocean, SST run. Contour interval is 1 gm-cal/cm^2-h. Solid lines are positive (upward) heat flux. Dashed lines are negative (downward) heat flux. (b) Differences in the sensible heat flux, control run minus SST run. Solid lines are positive indicating less energy available to the atmosphere in the SST run. Contour interval is 0.5 gm-cal/cm^2-h.

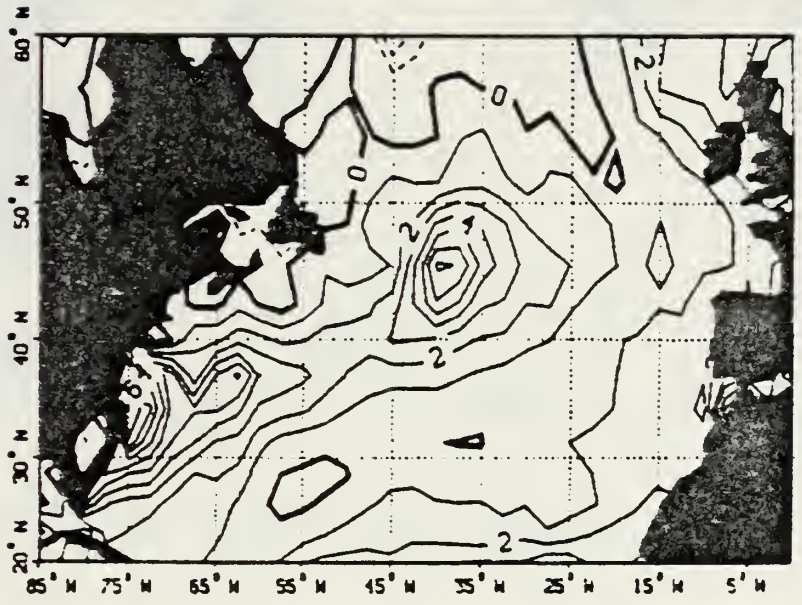

(a)

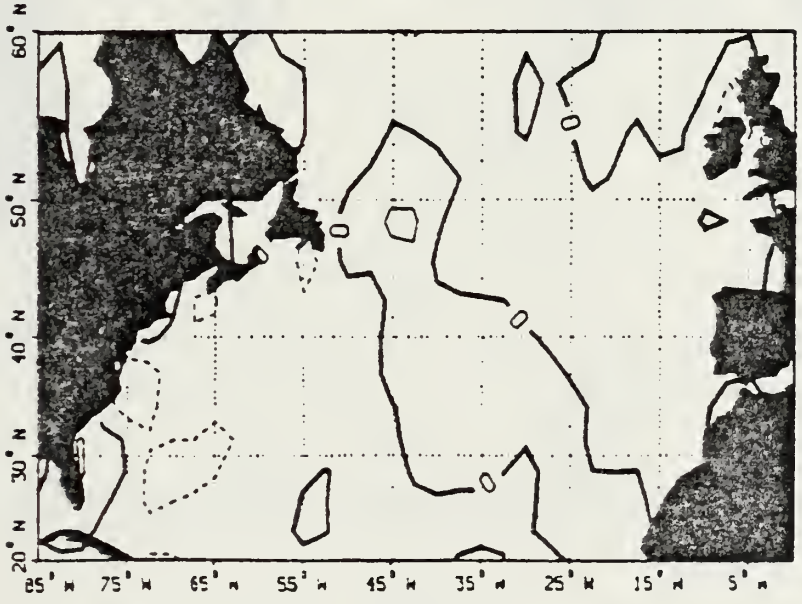

(b)

Figure 13. As in Fig. 12, except for the Atlantic Ocean.

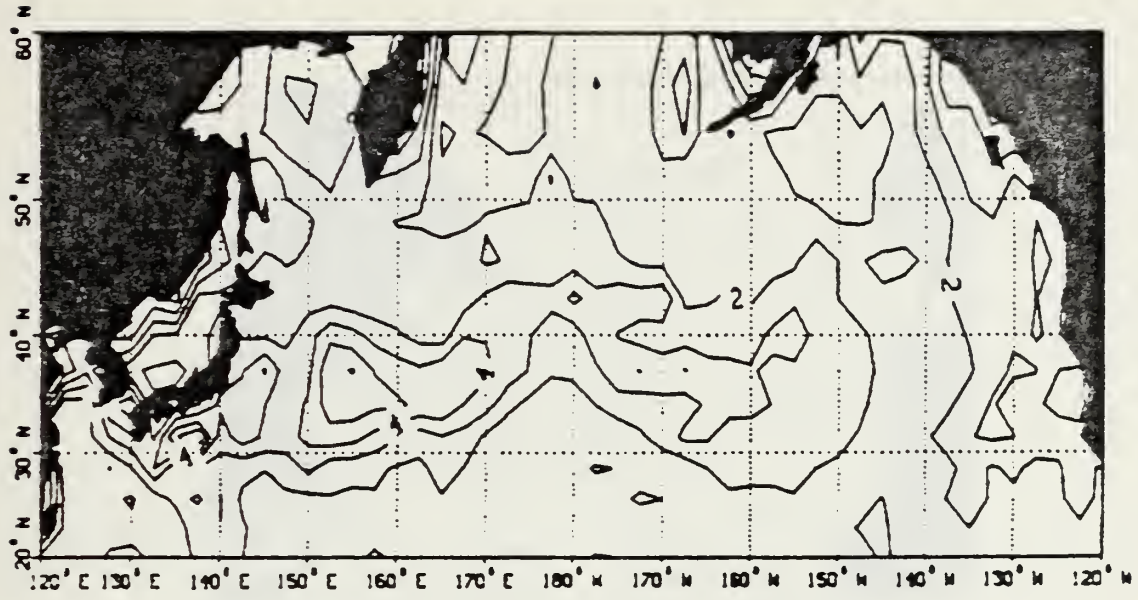

(a)

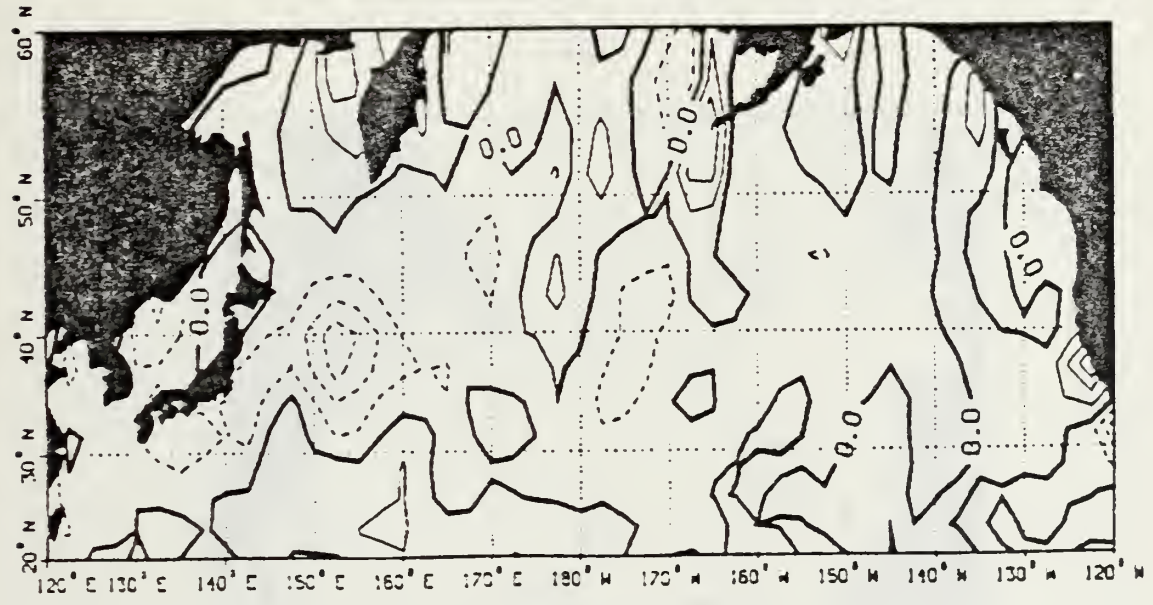

(b)

Figure 14. (a) The standard deviations of the sensible heat flux for the Pacific Ocean in the SST run. Contour interval is 1 gm-cal/cm^2-h. (b) The differences in the standard deviations of the two model runs, control run minus SST run. Contour interval is 0.5 gm-cal/cm^2-h.

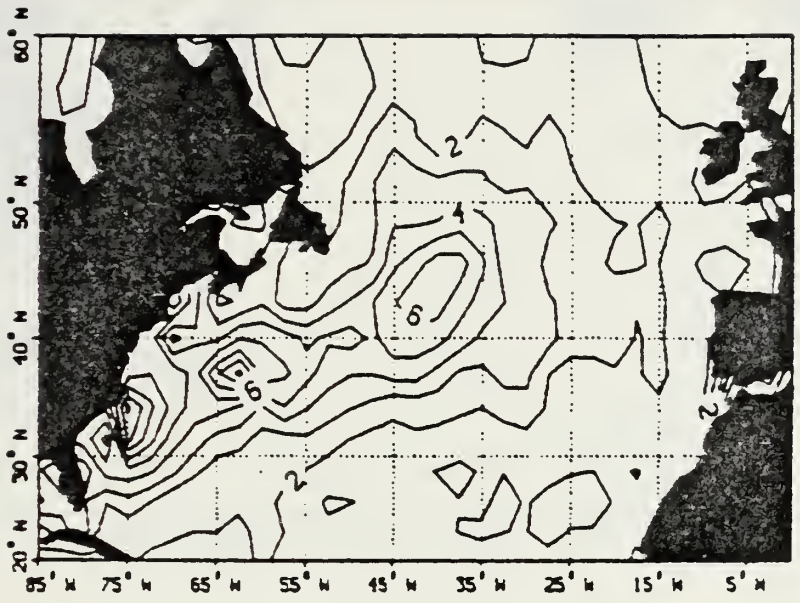

(a)

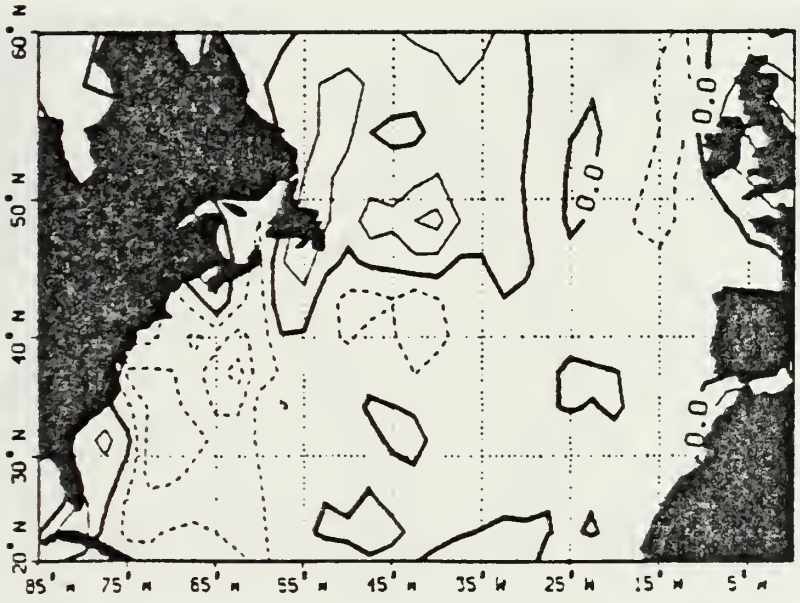

(b)

Figure 15. As in Fig. 14, except for the Atlantic Ocean.

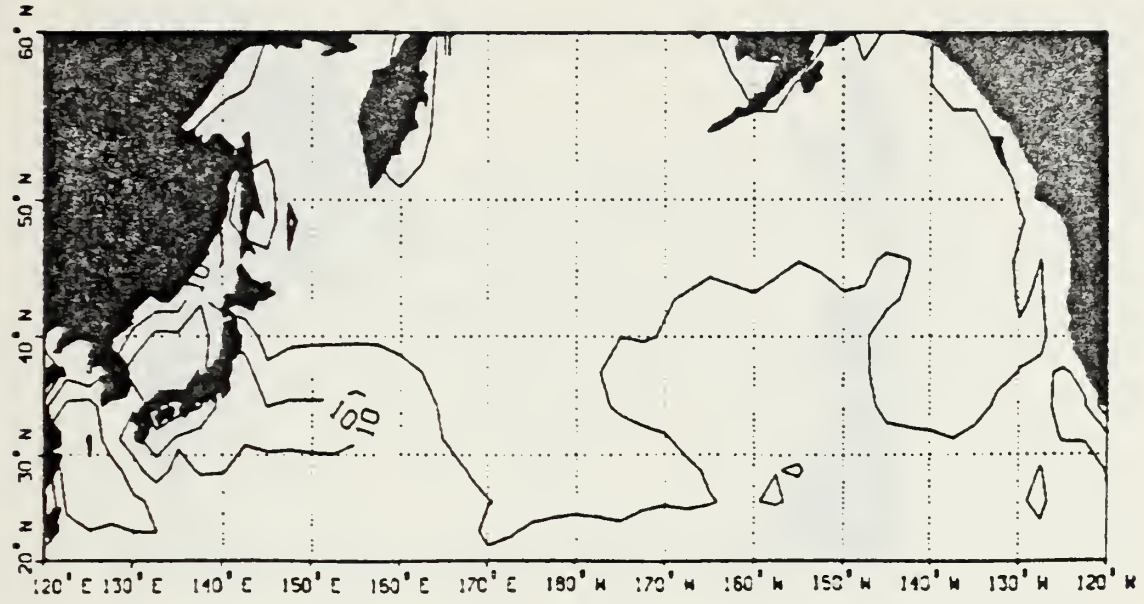

(a)

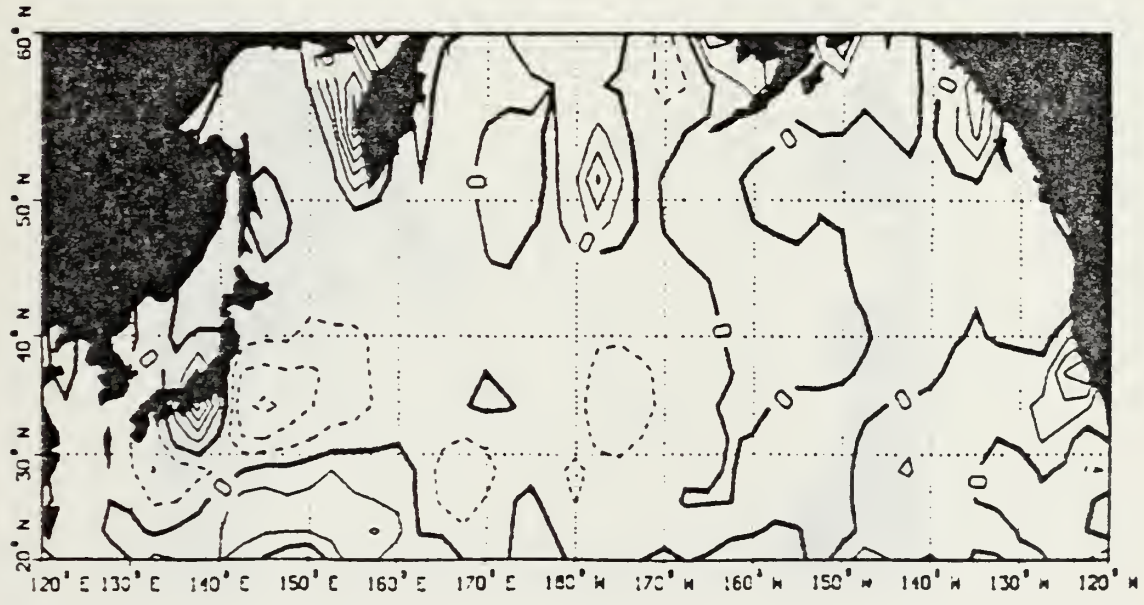

(b)

Figure 16. As in Fig. 12, except for the latent heat flux. (a) Contour interval is 5 gm-cal/cm^2-h. (b) Contour interval is 1 gm-cal/cm^2-h.

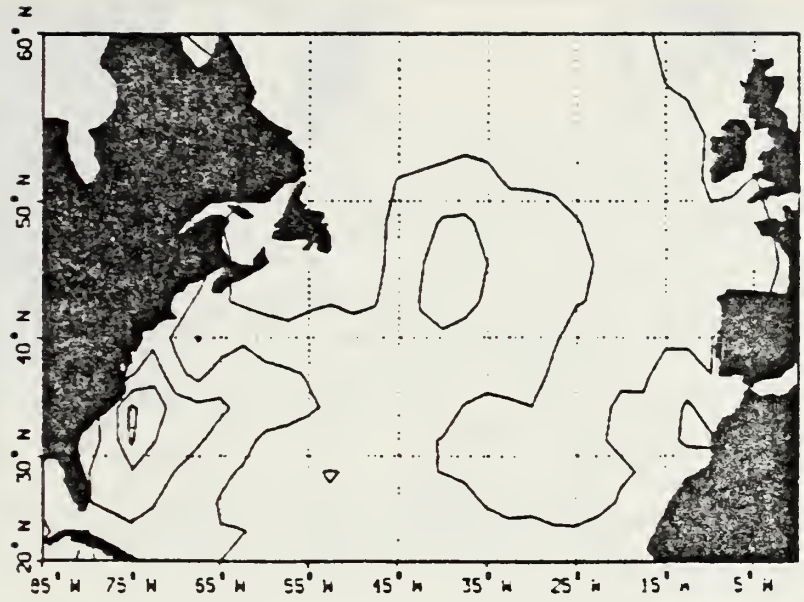

(a)

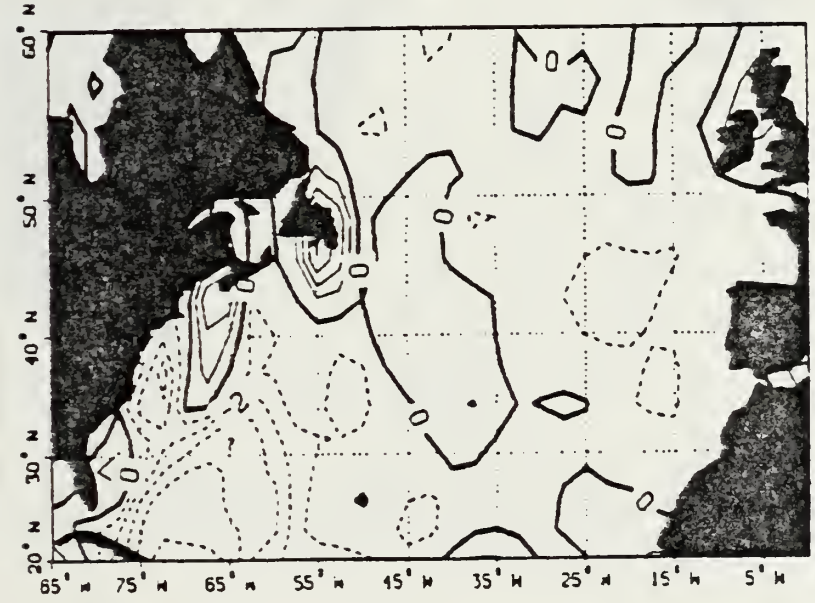

(b)

Figure 17. As in Fig. 12, except for the latent heat flux in the Atlantic Ocean. (a) Contour interval is 5 gm-cal/cm^2-h. (b) Contour interval is 1 gm-cal/cm^2-h.

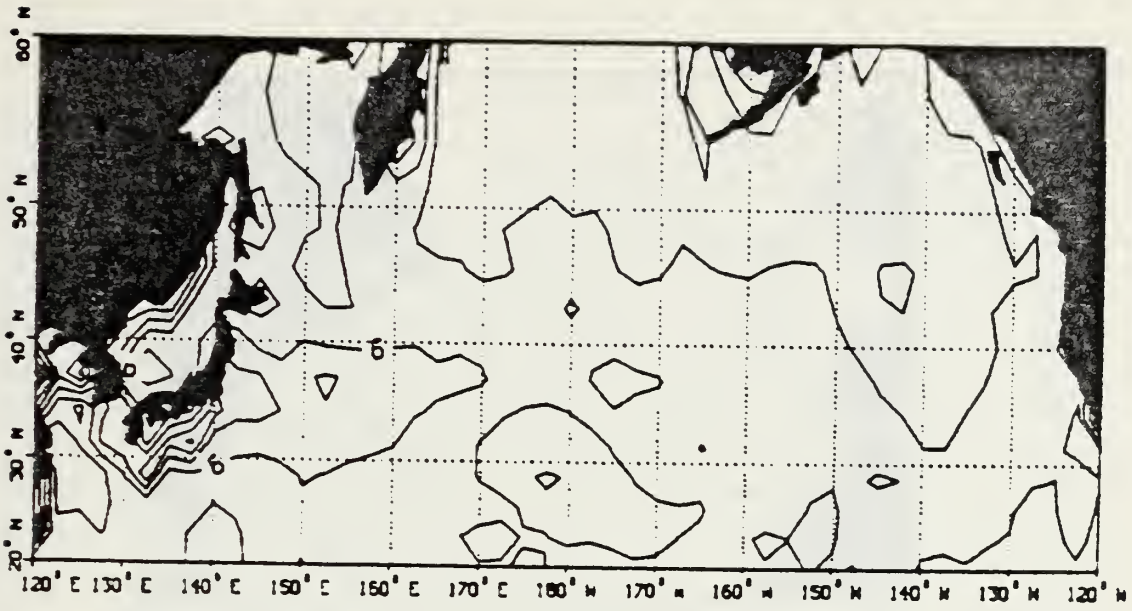

(a)

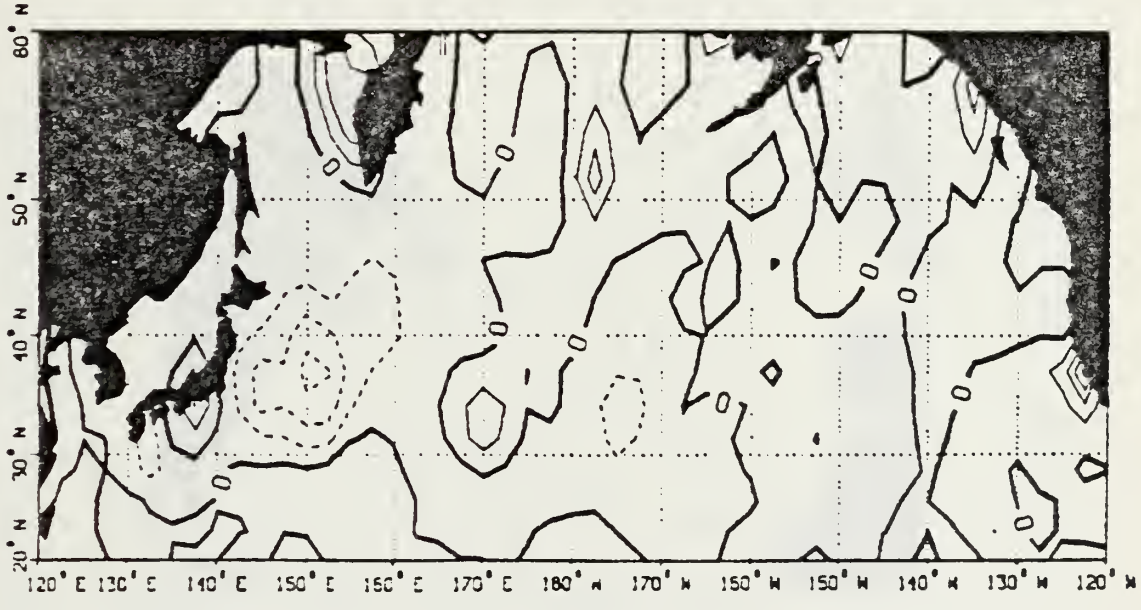

(b)

Figure 18. As in Fig. 14, except for the latent heat flux. (a) Contour interval is 3 gm-cal/cm^2-h. (b) Contour interval is 1 gm-cal/cm^2-h.

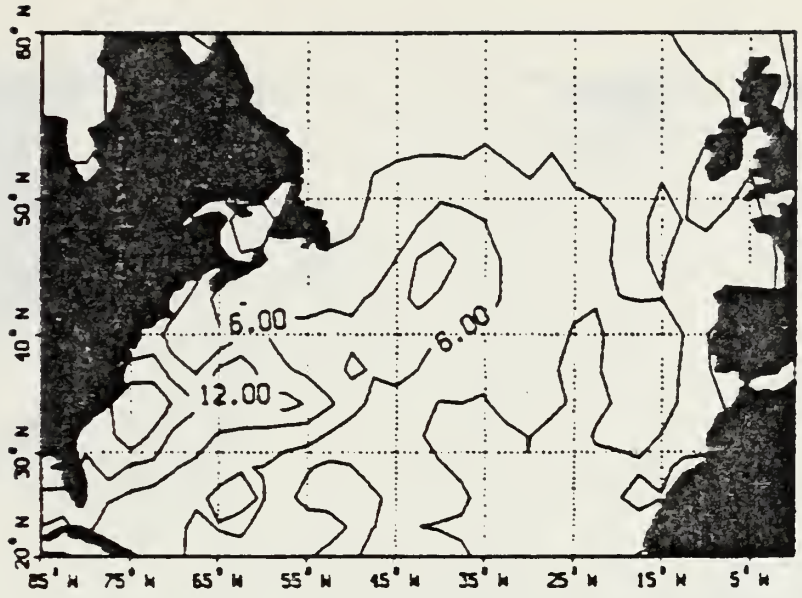

(a)

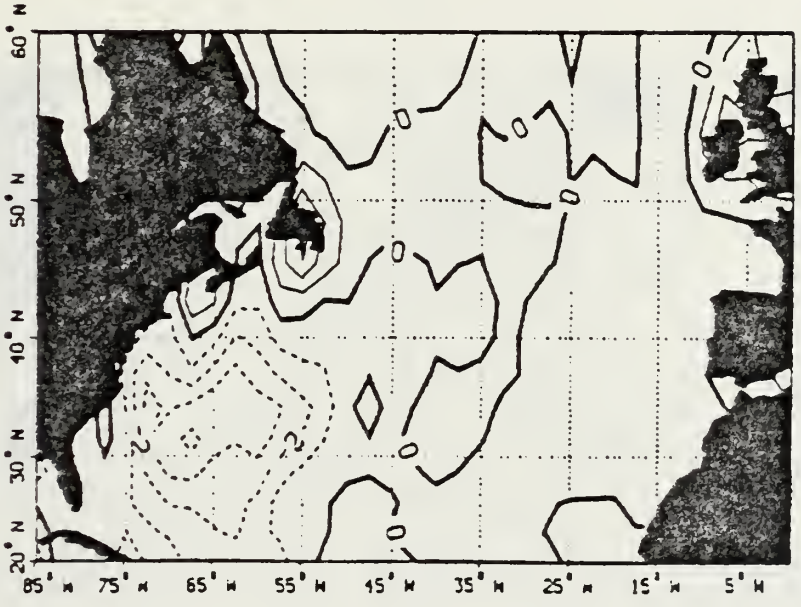

(b)

Figure 19. As in Fig. 14, except for the latent heat flux in the Atlantic Ocean. (a) Contour interval is 3 gm-cal/cm^2-h. (b) Contour interval is 1 gm-cal/cm^2-h.

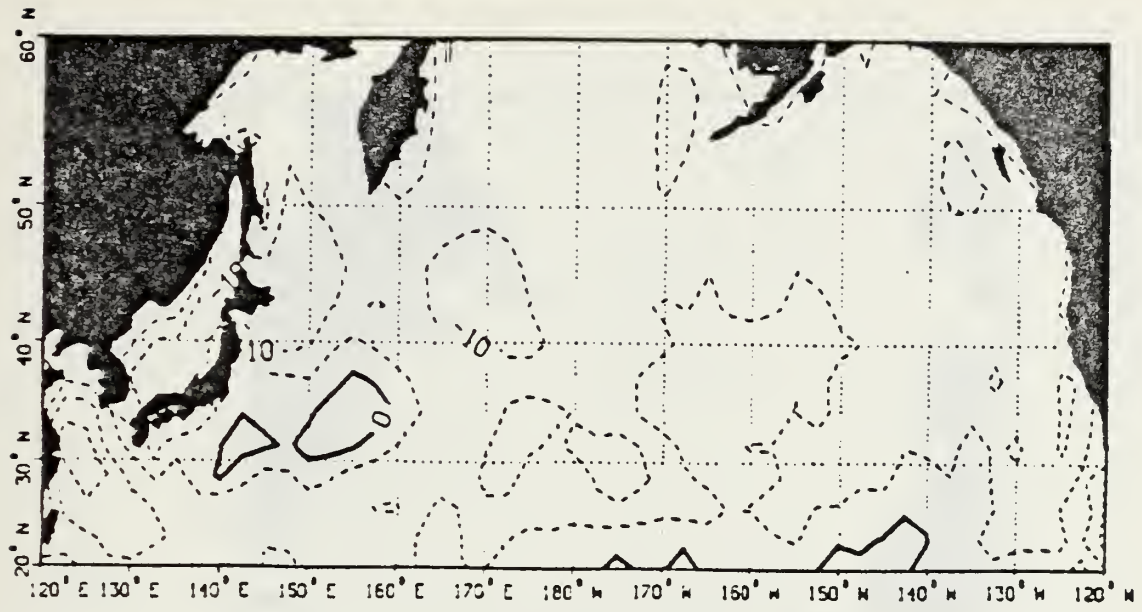

(a)

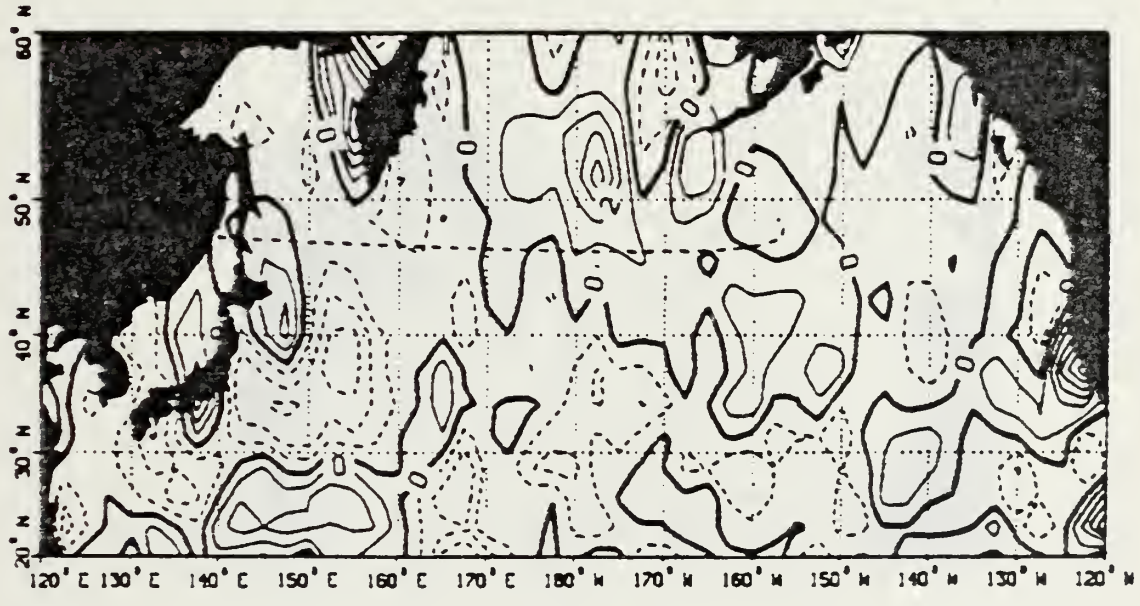

(b)

Figure 20. As in Fig. 12, except for the total heat flux.
(a) Contour interval is 5 gm-cal/cm^2-h.
(b) Contour interval is 1 gm-cal/cm^2-h.

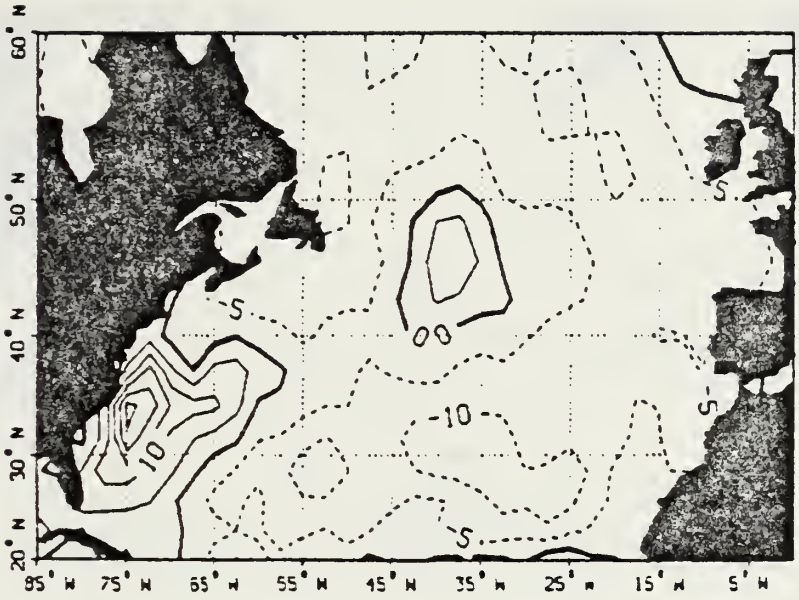

(a)

(b)

Figure 21. As in Fig. 12, except for the total heat flux in the Atlantic Ocean. (a) Contour interval is 5 gm-cal/cm^2-h. (b) Contour interval is 1 gm-cal/cm^2-h.

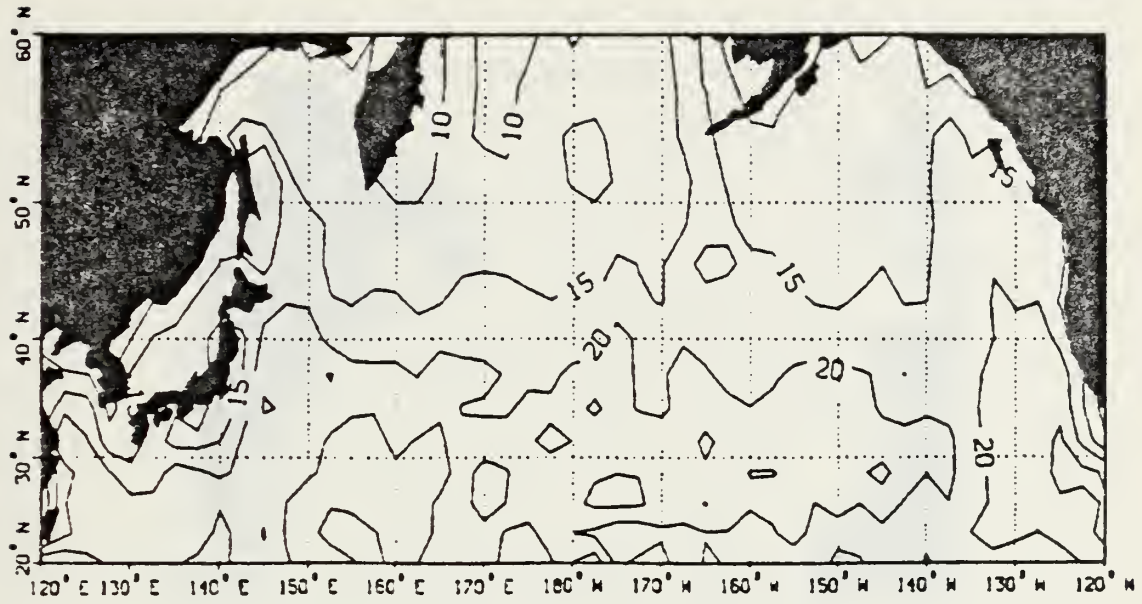

(a)

(b)

Figure 22. As in Fig. 14, except for the total heat flux.
(a) Contour interval is 5 gm-cal/cm^2-h.
(b) Contour interval is 0.5 gm-cal/cm^2-h.

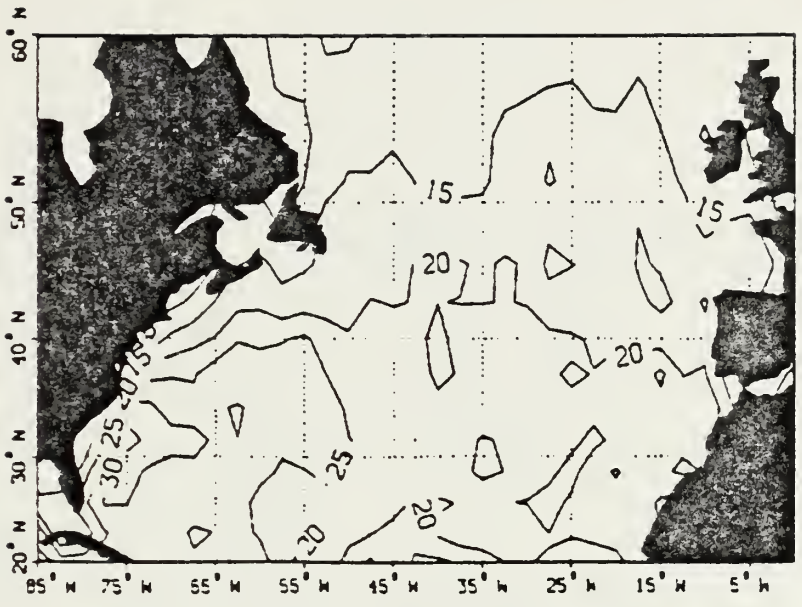

(a)

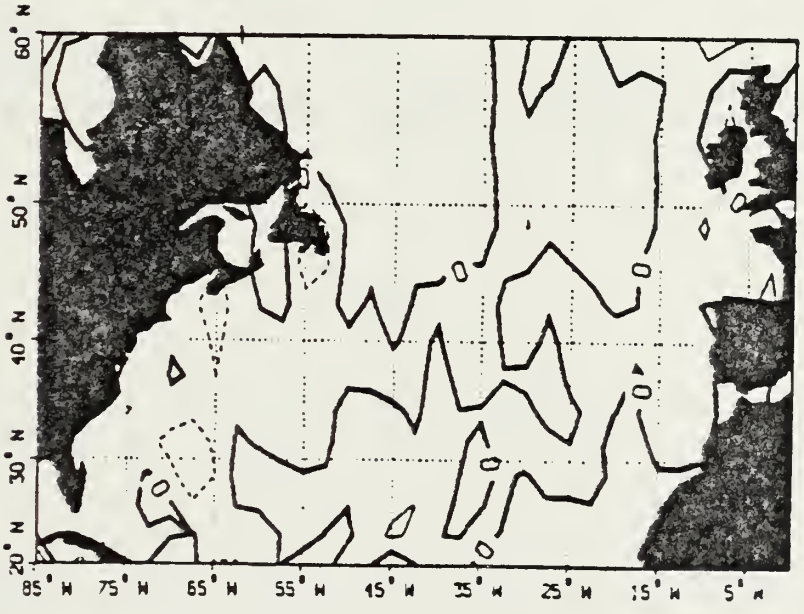

(b)

Figure 23. As in Fig. 14, except for the total heat flux in the Atlantic Ocean. (a) Contour interval is 5 gm-cal/cm^2-h. (b) Contour interval is 1 gm-cal/cm^2-h.

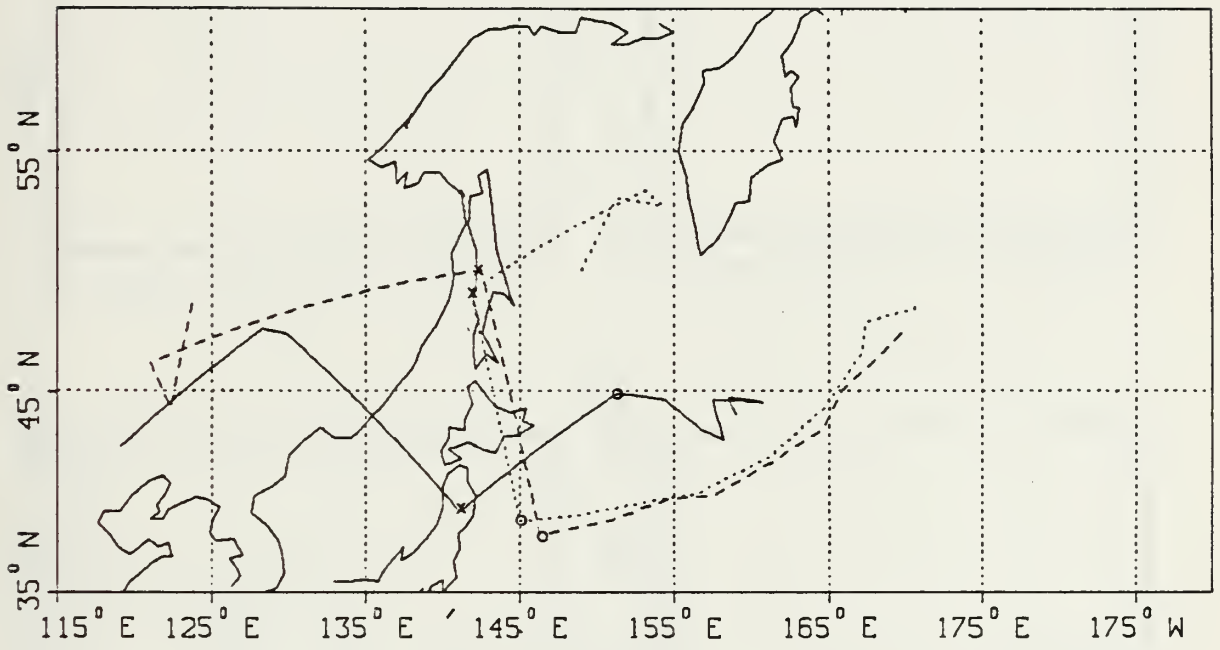

Figure 24. Tracks for storm P4. Solid is analysis, dashed is control run and dotted is SST run. "x" indicates position at 126 h. "o" indicates position at 138 h.

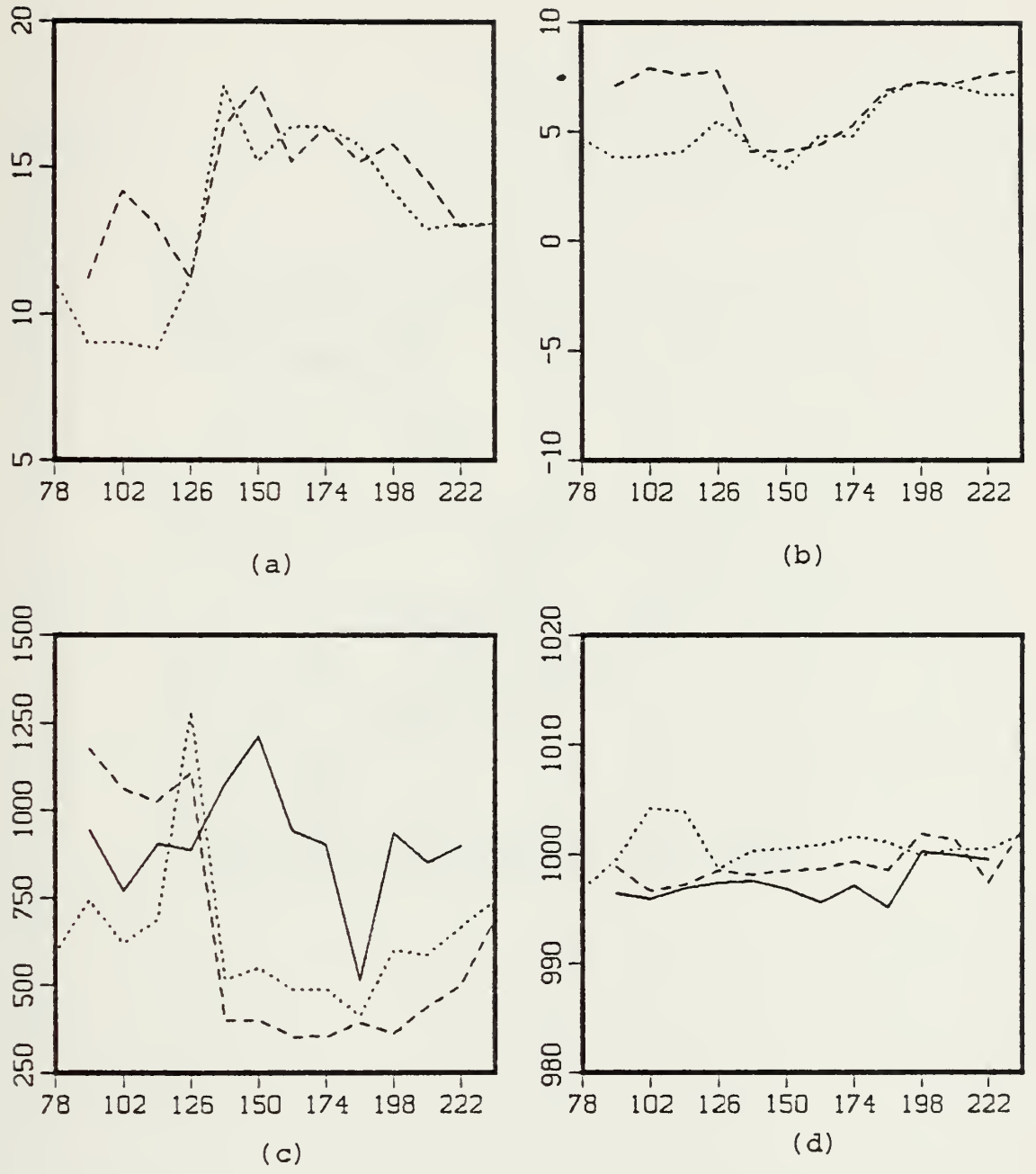

Figure 25. Storm parameters for the storm P4. (a) SST at storm center in °C. (b) Heat flux at storm center in gm-cal/cm^2-h. (c) Radius of storm in km. (d) Central pressure in mb. Solid is analysis, dashed is control run and dotted is SST run.

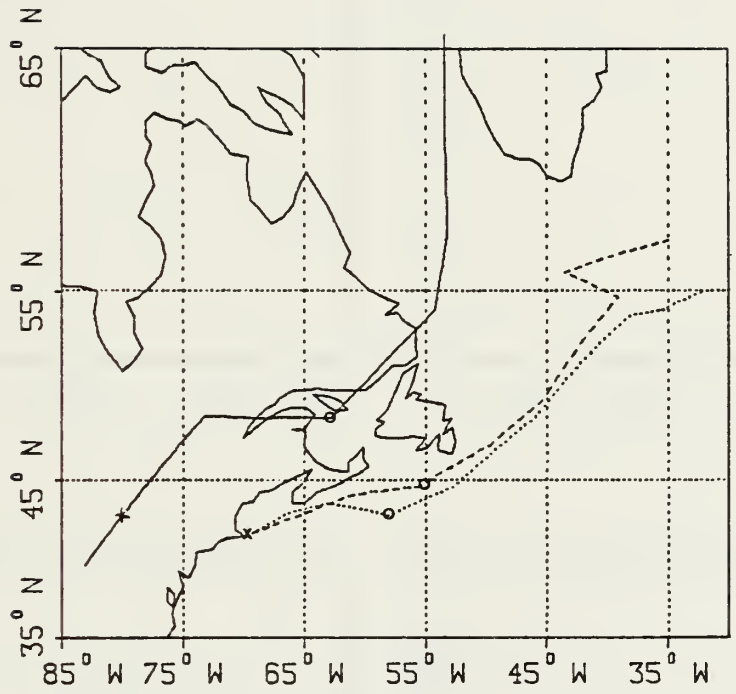

Figure 26. As in Fig. 24 except for storm A2. "x" indicates position at 126 h. "o" indicates position at 162 h.

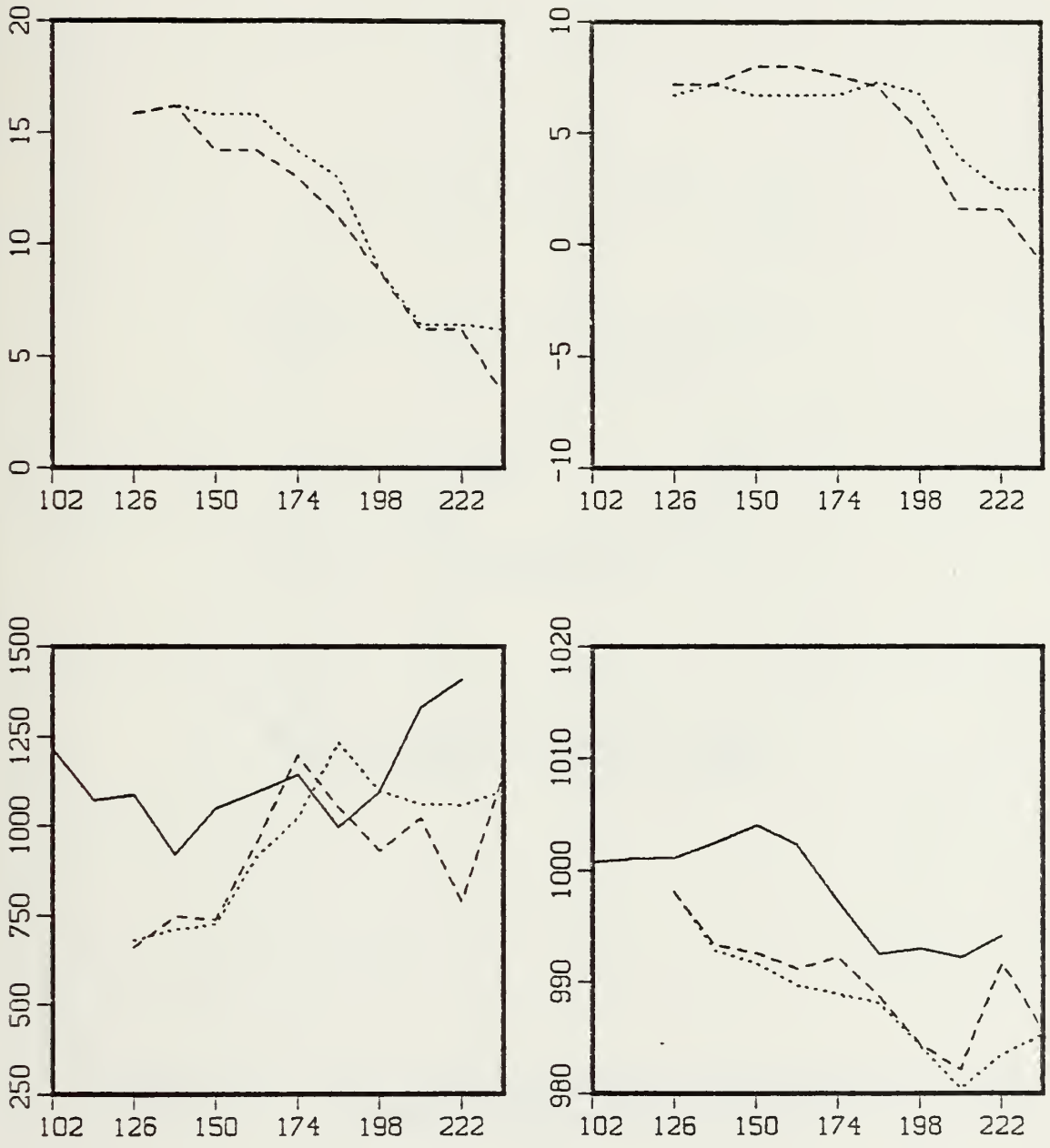

Figure 27. As in Fig. 25 except for storm A2.

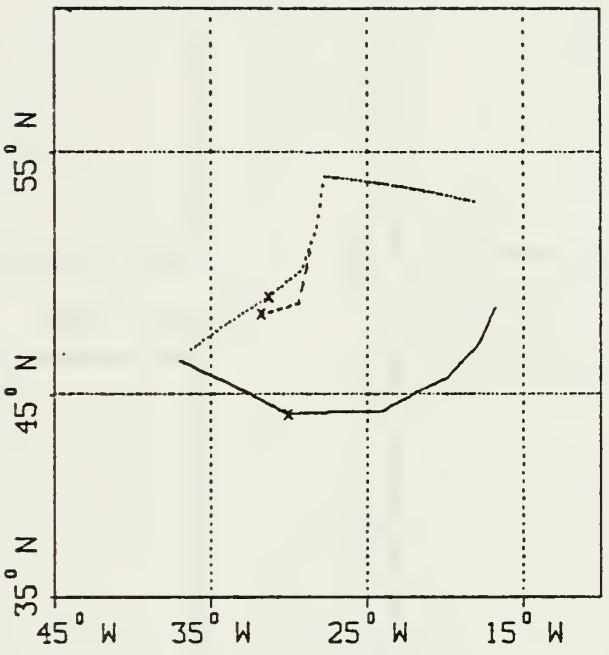

Figure 28. As in Fig. 24 except for storm A3. "x" indicates position at 138 h.

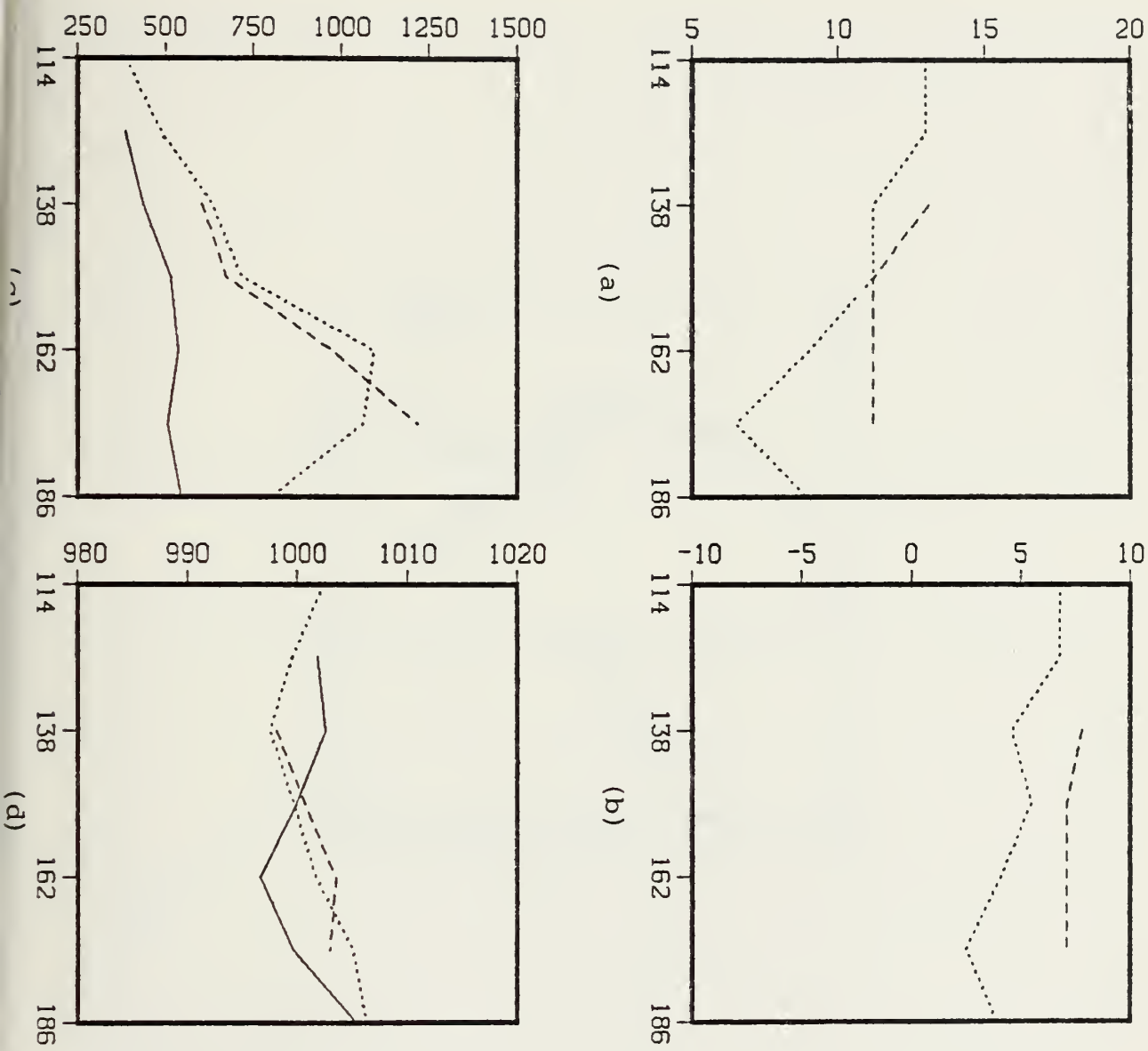

Figure 29. As in Fig. 25 except for storm A3.

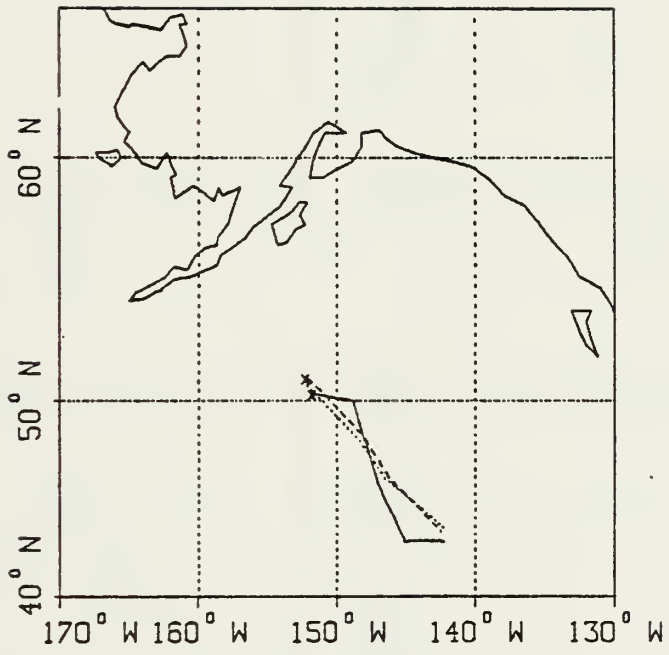

Figure 30. As in Fig. 24 except for storm P1. "x" indicates position at 6 h.

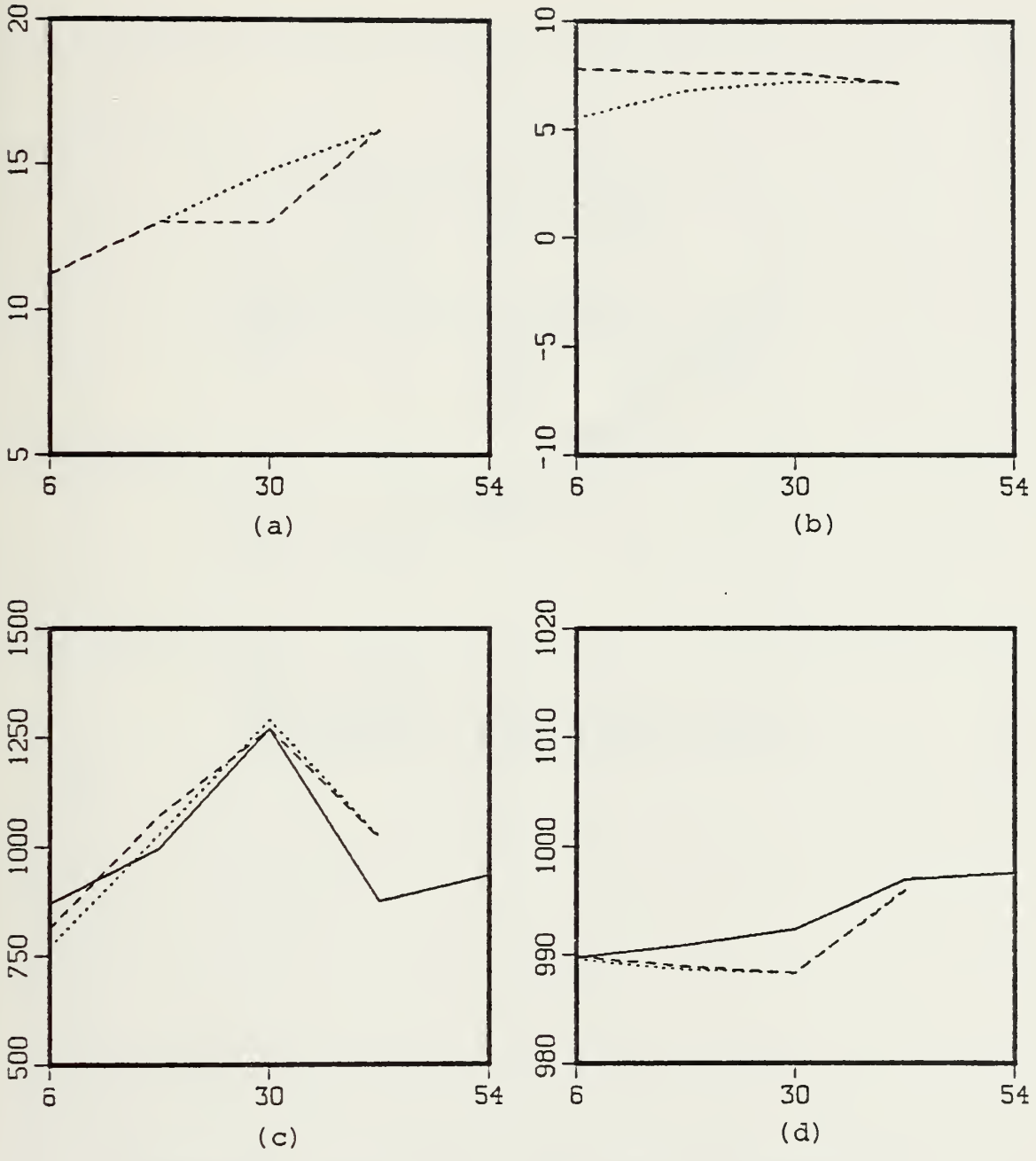

Figure 31. As in Fig. 25 except for storm P1.

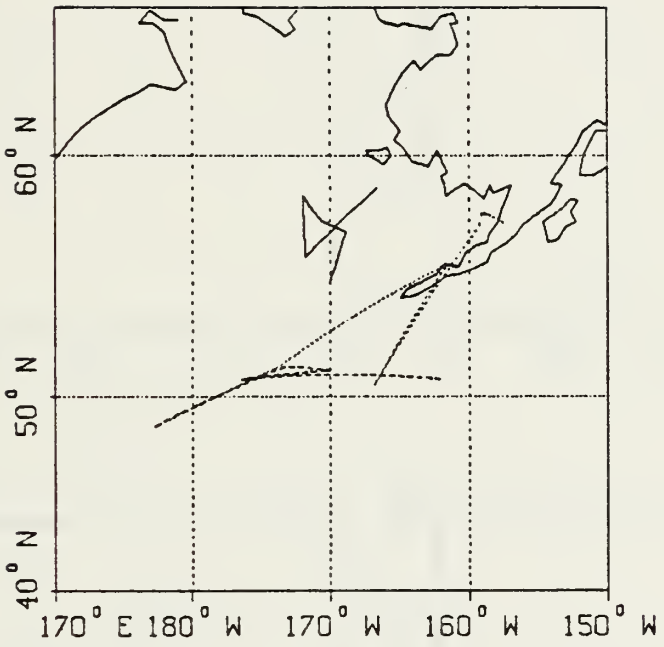

Figure 32. As in Fig. 24 except for storm P2.

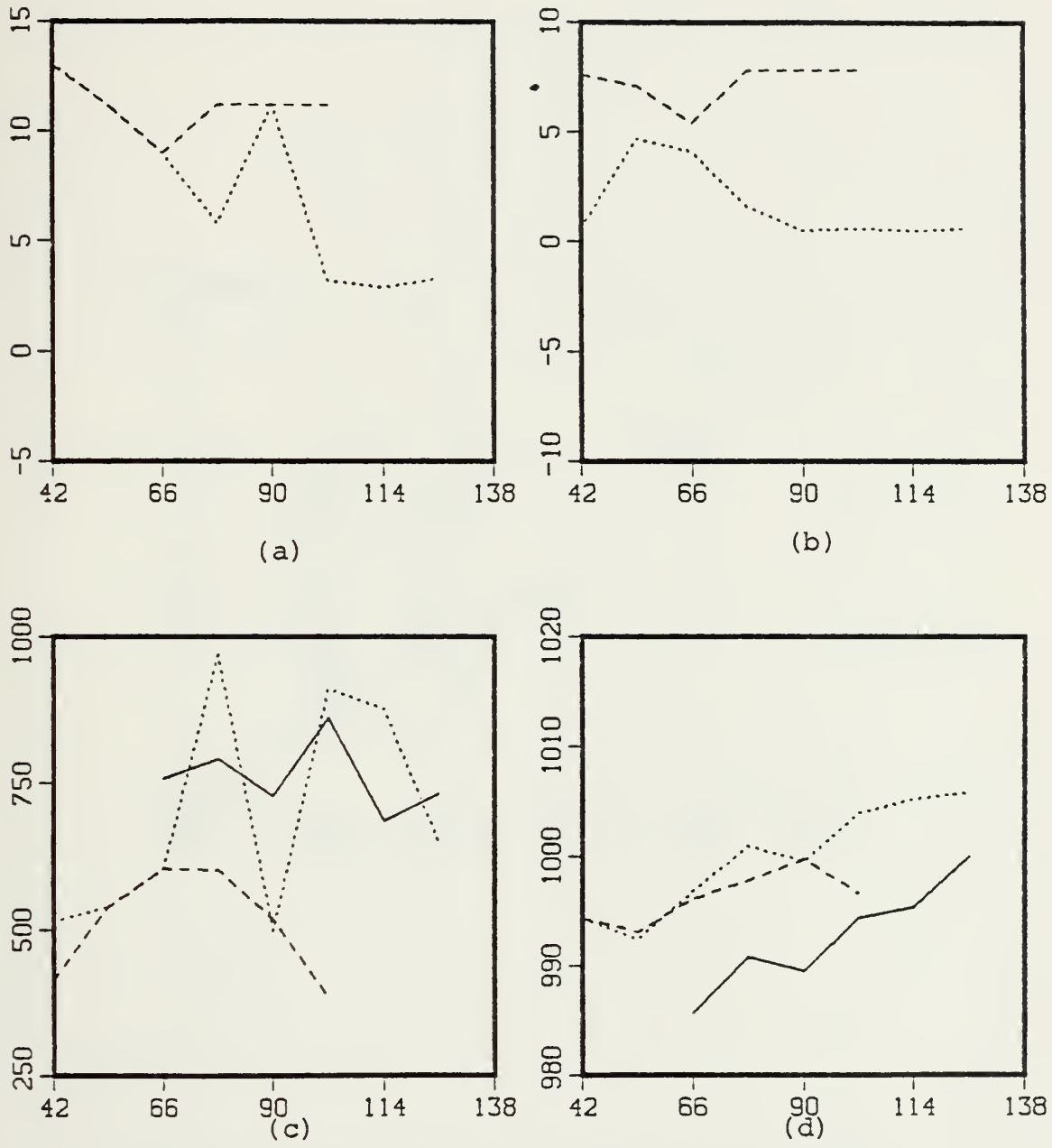

Figure 33. As in Fig. 25 except for storm P2.

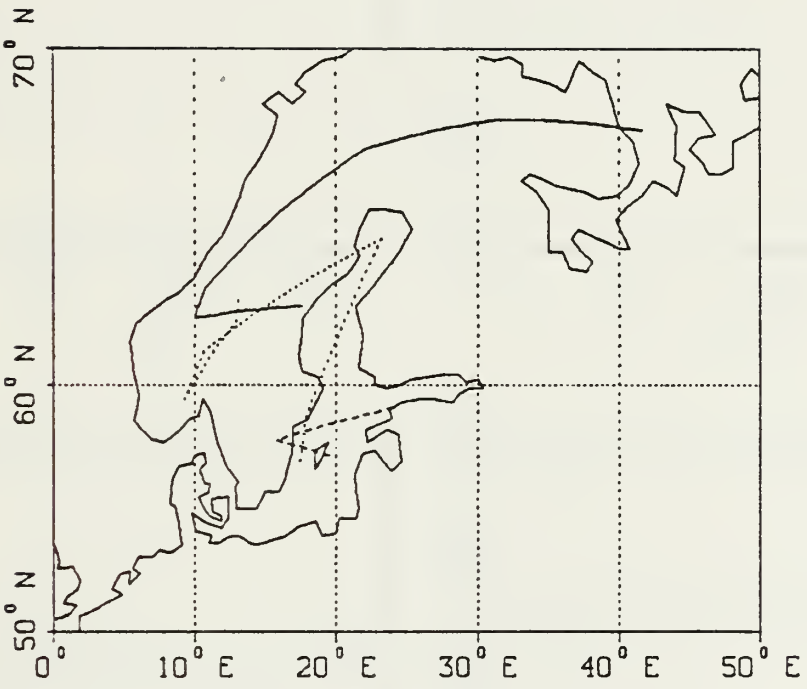

Figure 34. As in Fig. 24 except for storm A1.

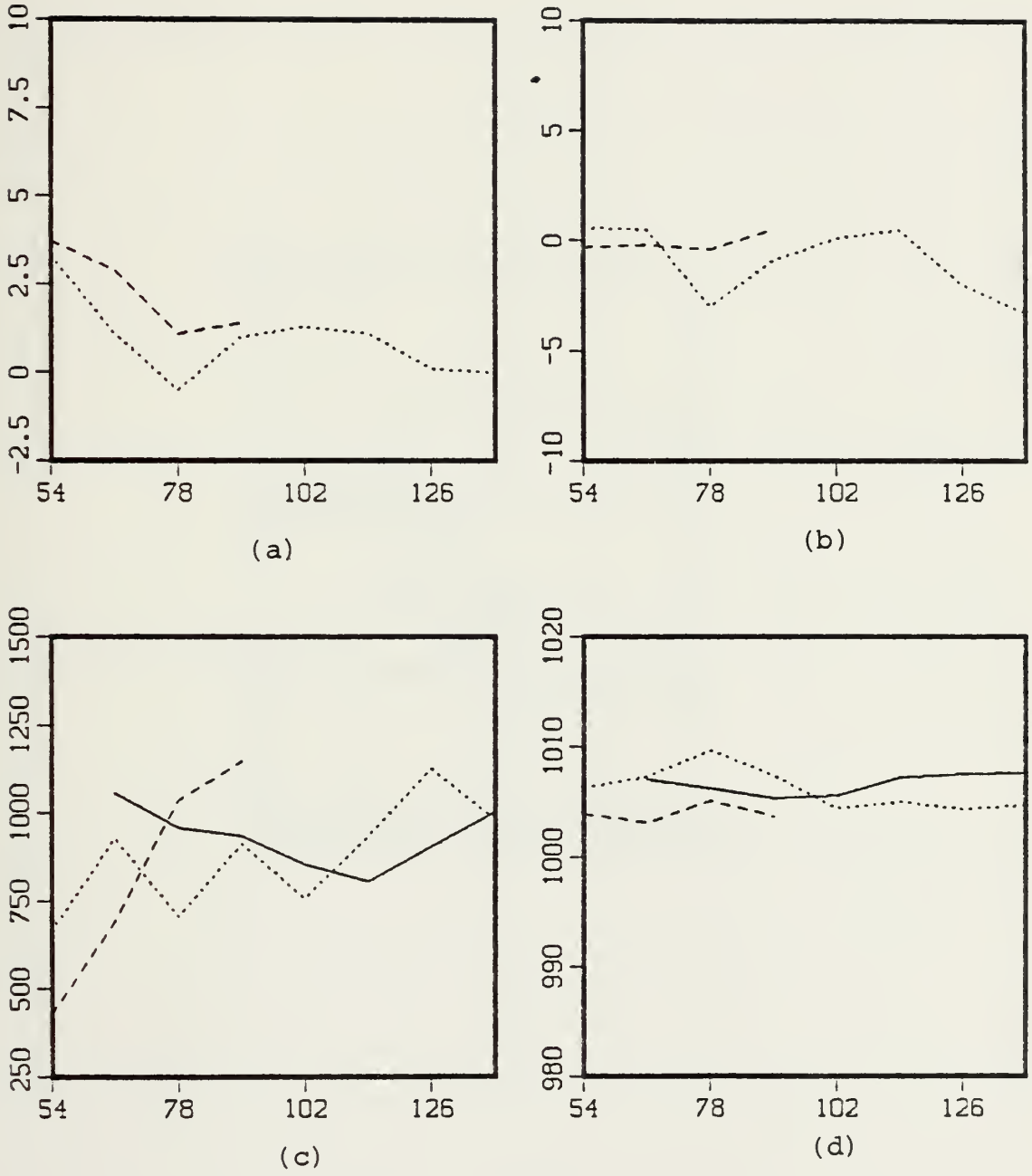

Figure 35. As in Fig. 25 except for storm A1.

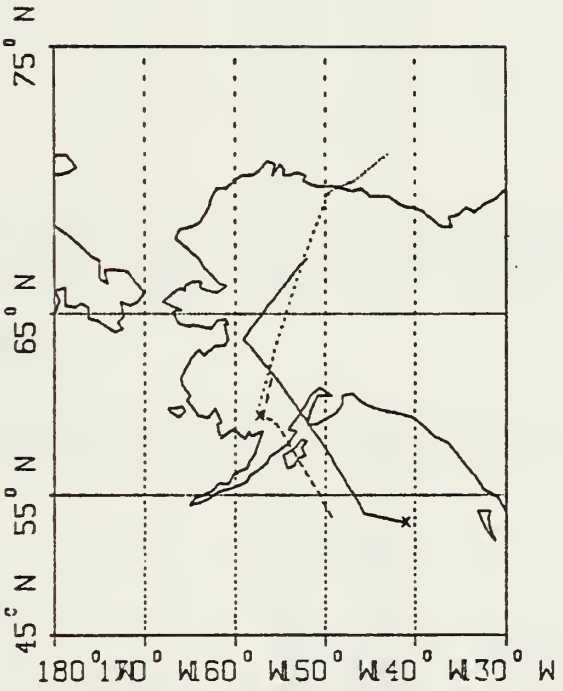

Figure 36. As in Fig. 24 except for storm P3. "x" indicates position at 90 h.

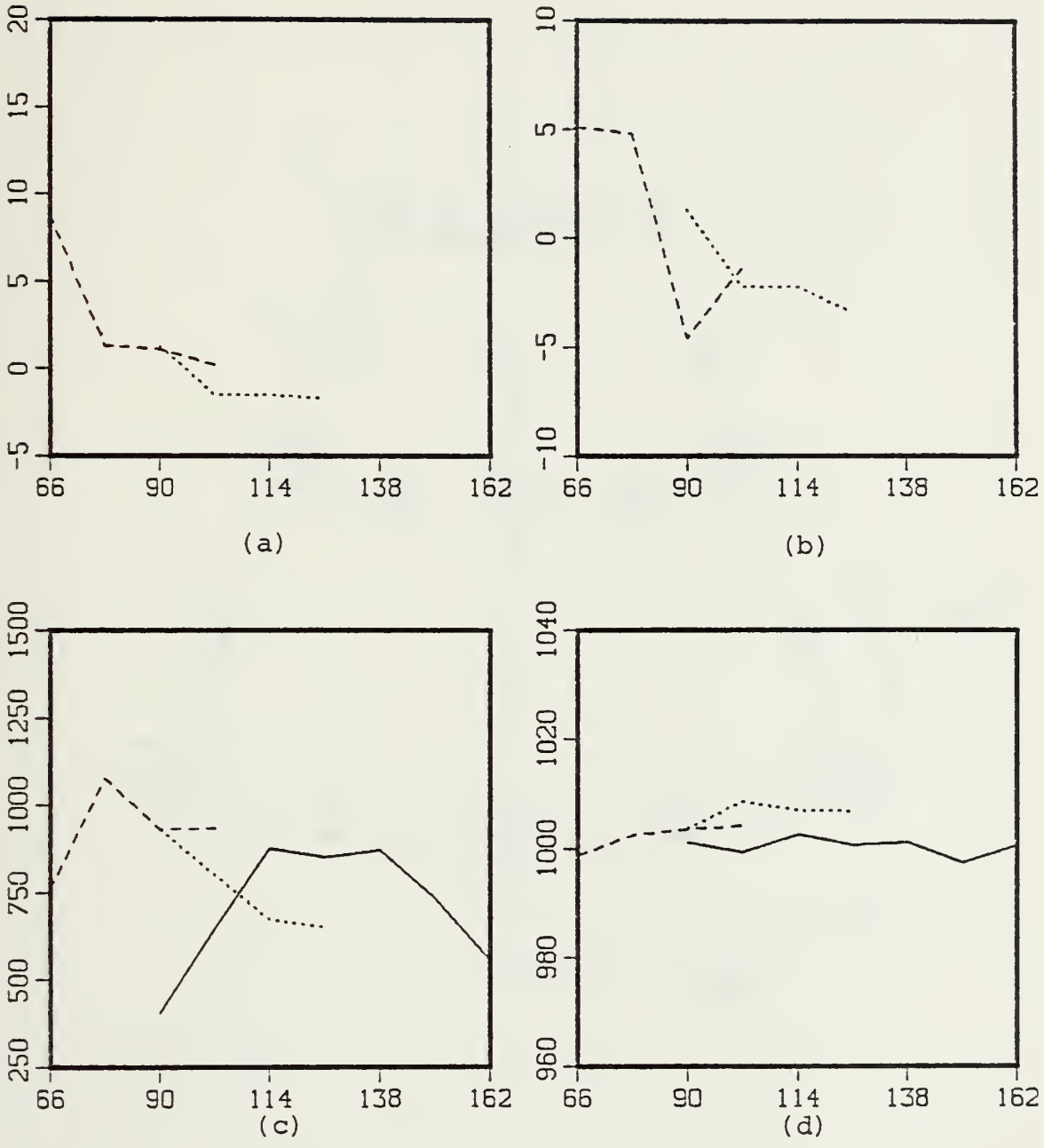

Figure 37. As in Fig. 25 except for storm P3.

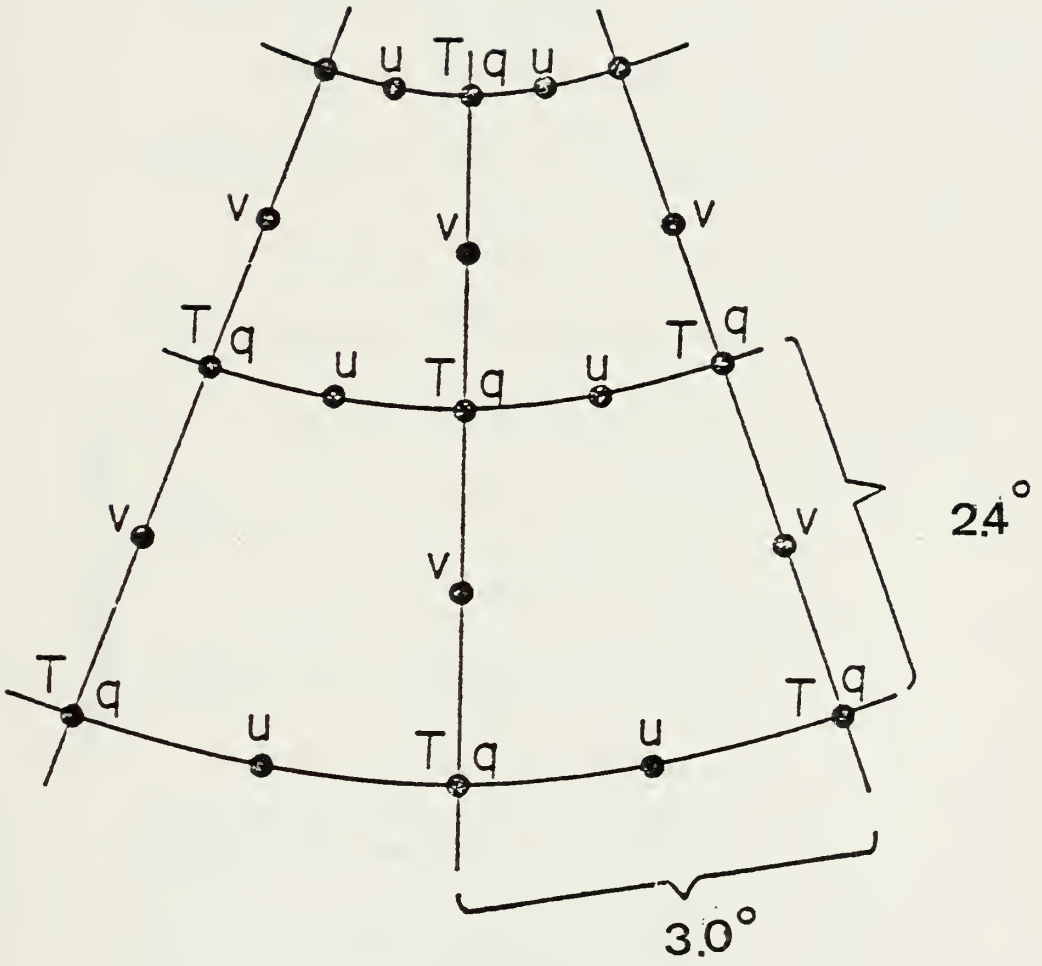

Figure 38. Horizontal distribution of model large-scale prognostic variables. $\dot{\sigma}$ which is not shown is carried at T points. [Sandgathe, 1981]

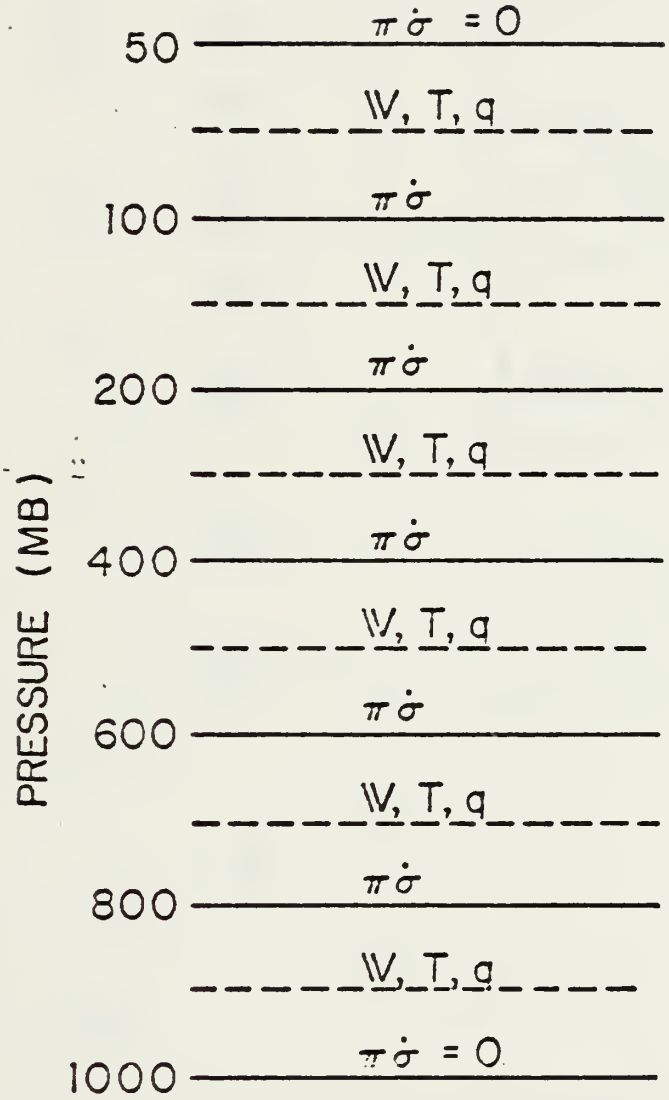

Figure 39. Vertical distribution of model large-scale prognostic variables. Pressure values of sigma levels vary with surface pressure. A surface pressure of 1000 mb is assumed in this figure. [Sandgathe, 1981]

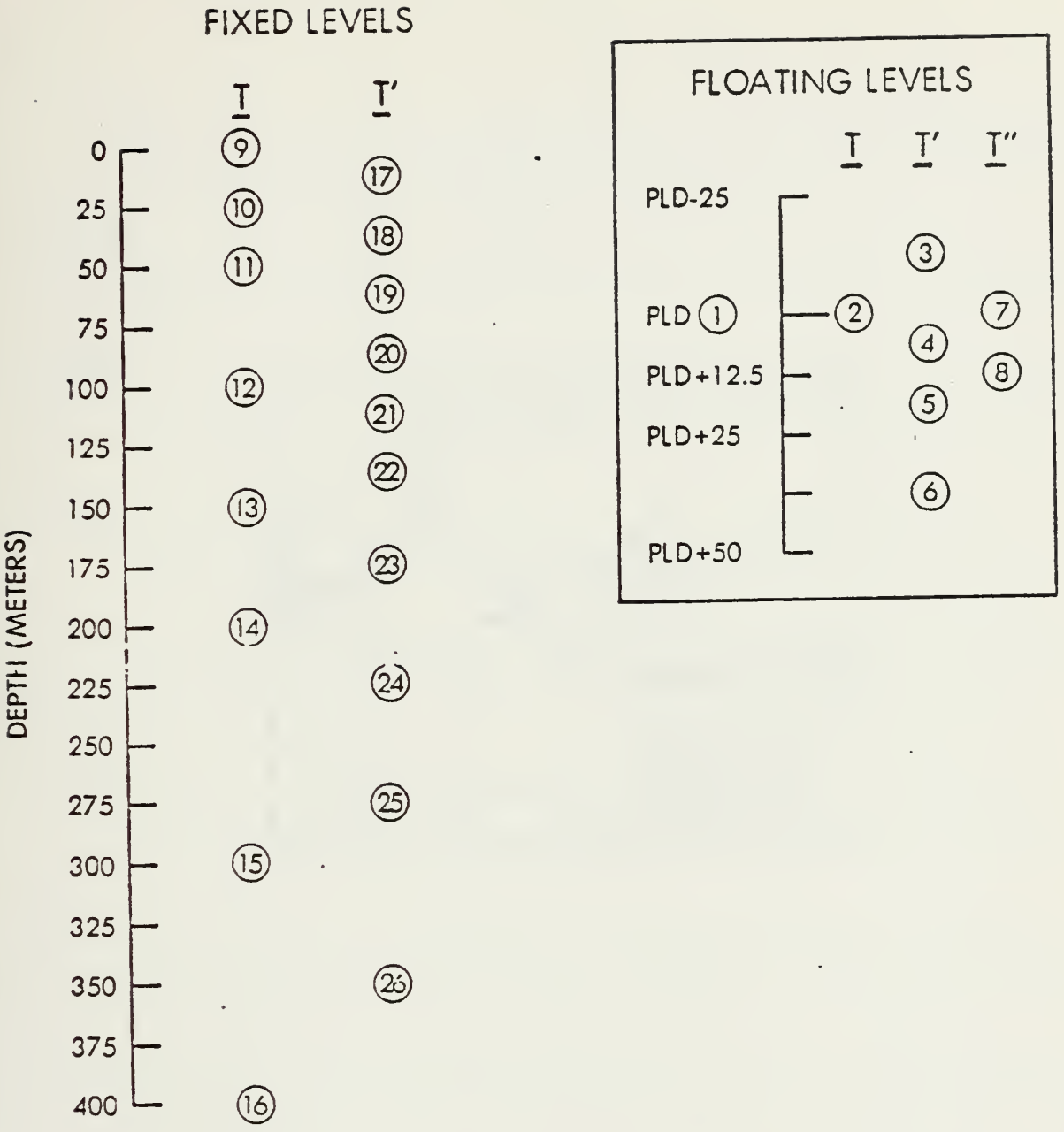

Figure 40. The twenty-six TOPS-EOTS ocean thermal structure parameters. Labeled T, T' and T" are temperature, first vertical temperature difference and second vertical temperature difference, respectively. Parameters 2-8 are associated with floating levels defined relative to parameter 1, Primary Layer Depth (PLD). Parameters 9-26 are associated with fixed levels. [Clancy and Pollack, 1982]

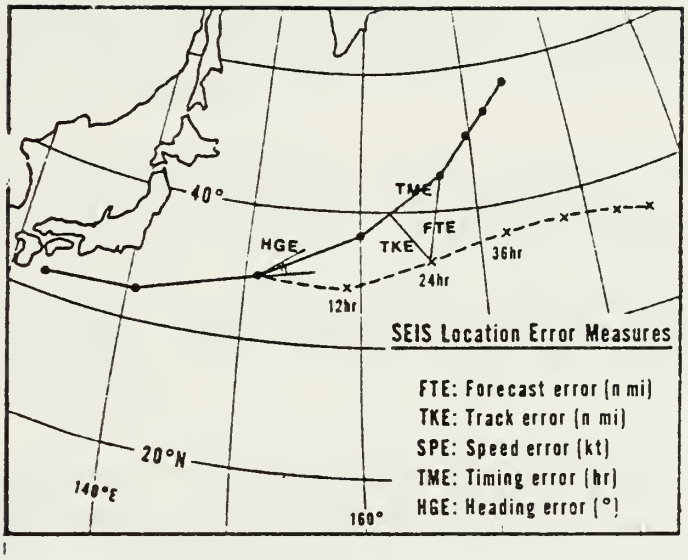

Figure 41. SEIS derived location errors measures. [Harr, et al., 1983]

LIST OF REFERENCES

Arakawa, A., and V. Lamb, 1977: Computational design of the basic dynamical processes of the UCLA general circulation model. Methods in Computational Physics, 17, 173-265, Academic Press, New York.

Arakawa, A., and W.H. Schubert, 1974: Interaction of a cumulus cloud ensemble with the large scale environment, Part I. J. Atmos. Sci., 31, 674-701.

Arpe, K.V., 1981: Impact of sea-surface temperature anomaly on medium-range weather forecasts. Unpublished report, European Centre for Medium-Range Weather Forecasts, 8 pages plus 14 figures.

Camp, N.T., and R.L. Elsberry, 1978: Oceanic thermal response to strong atmospheric forcing II. The role of one-dimensional processes. J. Phys. Oceanogr., 8, 215-224.

Clancy, R.M., and P.J. Martin, 1979: The NORDA/FLENUMOCEANCEN thermodynamical ocean prediction system (TOPS): A technical description. NORDA Tech. Note 54, NORDA, NSTL Station MS, 28 pp.

Clancy, R.M., 1981: The Expanded Ocean Thermal Structure (EOTS) Analysis: Description, critique and outlook. Paper presented at Ocean Prediction Workshop. 29 April-2 May, 1981, Monterey, CA.

Clancy, R.M., P.J. Martin, S.A. Piacsek and K.D. Pollak, 1981: Test and evaluation of an operationally capable synoptic upper ocean forecast system. NORDA Tech. Note 92, NORDA NSTL Station, MS., 67 pp.

Clancy, R.M., and K.D. Pollack, 1983: A real time Synoptic ocean thermal analysis/forecast system. Prog. Oceanogr., 12, 383-424.

Deardorff, J.W., 1972: Parameterization of the planetary boundary layer for use in general circulation models. Mon. Wea. Rev., 100, 93-106.

Elsberry, R.L., and N.T. Camp, 1978: Oceanic thermal response to strong atmospheric forcing. Part I. Characteristics of forcing events. J. Phys. Oceanogr., 8, 206-214.

Elsberry, R.L., and S.D. Raney, 1978: Sea-surface temperature response to variations in atmospheric wind forcing. J. Phys. Oceanogr., 8, 881-887.

Elsberry, R.L., R.L. Haney, R.T. Williams, R.S. Bogart, H.D. Hamilton and E.F. Hinson, 1982: Ocean/troposphere/stratosphere forecast systems: a state-of-the-art review. Technical Report CR 8204, Systems and Applied Sciences Corporation, 570 Casanova Ave., Monterey, CA., 79 pp.

Harr, P.A., T.L. Tsui and L.R. Brody, 1983: Model verification statistics tailored for the field forecaster. Preprint volume, Seventh Conference on Numerical Weather Prediction, Omaha, NE., published by the American Meteorological Society, Boston, MA., 241-246.

Holl, M.M., and B.R. Mendenhall, 1971: Fields by information blending, sea level pressure version. Tech. Rept. M167, Meteorology International Inc., 2600 Garden Road, Suite 145, Monterey CA., 71 pp.

Holl, M.M., M.J. Cumming and B.R. Mendenhall, 1979: The expanded ocean thermal structure analysis system: A development based on the fields by information blending methodology. Tech. Rept. M241, Meteorology International Inc., 2600 Garden Road, Suite 145, Monterey, CA., 216 pp.

Katayama, A., 1972: A simplified scheme for computing radiative transfer in the troposphere. Technical Report No. 6, Dept. of Meteorology, UCLA.

Lord, S.J., 1978: Development and observational verification of a cumulus cloud parameterization. Ph.D. Thesis, Dept. of Atmos. Sci., UCLA.

Mellor, G.L., and T. Yamada, 1974: A hierarchy of turbulence closure models for planetary boundary layers. J. Atmos. Sci., 31, 1791-1806.

Mendenhall, B.R., M.J. Cumming and M.M. Holl, 1978: The expanded ocean thermal structure analysis system user's manual. Tech. Rept. M232, Meteorology International Inc., 2600 Garden Road, Suite 145, Monterey, CA., 71 pp.

Randall, D.A., 1976: The interaction of the planetary boundary layer with large scale circulations. Ph.D. Thesis, Dept. of Atmos. Sci., UCLA.

Rosmond, T.E., 1981: NOGAPS: Navy operational global atmospheric prediction system. Preprint volume, Fifth Conference on Numerical Weather Prediction, Monterey, CA., published by the American Meteorological Society, Boston, MA., 7479.

Rosmond, T.E., A.L. Weinstein and S.A. Piacsek, 1983: Coupled ocean-atmosphere modeling for 3-15 day numerical prediction: A workshop report. NEPRF Tech. Rept. TR 8305, NEPRF, Monterey, CA., 81 p.

Sanders, F., and J.R. Gyakum, 1980: Synoptic dynamic climatology of the "bomb." Mon. Wea. Rev., 108, 1589-1606.

Sandgathe, S.A., 1981: A numerical study of the role of air-sea fluxes in extratropical cyclogenesis. Ph.D. Thesis, Dept. of Meteorology, Naval Postgraduate School, Monterey, CA.

Schlesinger, M.E., 1976: A numerical simulation of the general circulation of the atmospheric ozone. Ph.D. Thesis, Dept. of Atmos. Sci., UCLA.

Williamson, D.L., 1981: Storm track representation and verification. Tellus, 33, 513-530.

INITIAL DISTRIBUTION LIST

		No. Copies
1.	Defense Technical Information Center Cameron Station Alexandria, VA 22314	2
2.	Library, Code 0142 Naval Postgraduate School Monterey, CA 93943	2
3.	Chairman, (Code 63Rd) Department of Meteorology Naval Postgraduate School Monterey, CA 93943	1
4.	Chairman, (Code 68Mr) Department of Oceanography Naval Postgraduate School Monterey, CA 93943	1
5.	Director Naval Oceanography Division Naval Observatory 34th and Massachusetts Avenue, NW Washington, D.C. 20390	1
6.	Commander Naval Oceanography Command NSTL Station Bay St. Louis, MS 39522	1
7.	Commanding Officer Naval Oceanographic Office NSTL Station Bay St. Louis, MS 39522	1
8.	Commanding Officer Fleet Numerical Oceanography Center Monterey, CA 93943	1
9.	Commanding Officer Naval Ocean Research and Development Activity NSTL Station Bay St. Louis, MS 39522	1

10. Commanding Officer — 1
Naval Environmental Prediction
Research Facility
Monterey, CA 93943

11. Chairman, Oceanography Department — 1
U.S. Naval Academy
Annapolis, MD 21402

12. Chief of Naval Research — 1
800 N. Quincy Street
Arlington, VA 22217

13. Professor R.L. Elsberry, Code 63Es — 3
Department of Meteorology
Naval Postgraduate School
Monterey, CA 93943

14. C.S. Liou, Code 63Lu — 1
Department of Meteorology
Naval Postgraduate School
Monterey, CA 93943

15. LCDR P.H. Ranelli — 3
USS New Jersey (BB-62)
Fleet Post Office
San Francisco, CA 96688

16. LCDR S.A. Sandgathe — 1
Joint Typhoon Warning Center
CONNAVMARIANAS Box 12
Fleet Post Office
San Francisco, CA 96630

17. LT. P.J. Rovero, Code 63 — 1
Department of Meteorology
Naval Postgraduate School
Monterey, CA 93943

18. Capt. A.R. Shaffer, Code 63 — 1
Department of Meteorology
Naval Postgraduate School
Monterey, CA 93943

19. Dr. T.E. Rosmond — 1
Naval Environmental Prediction
Research Facility
Monterey, CA 93943

20. Dr. T.L. Tsui — 1
Naval Environmental Prediction
Research Facility
Monterey, CA 93943

207551

Thesis
R2124 Ranelli
c.1 Response of an atmospheric prediction model to time-dependent sea-surface temperatures.